

## COARSE GRAINING IN SIMULATED CELL POPULATIONS

DIRK DRASDO

*Interdisciplinary Center for Bioinformatics (IZBI), University of Leipzig,  
Haertelstr. 16/18, D-04107 Leipzig, Germany  
drasdo@izbi.uni-leipzig.de*

and

*Max-Planck-Institute for Mathematics in the Sciences,  
Kreutzstr. 22-26, D-4103 Leipzig, Germany*

Received 16 November 2004

Revised 26 July 2005

The main mechanisms that control the organization of multicellular tissues are still largely open. A commonly used tool to study basic control mechanisms are *in vitro* experiments in which the growth conditions can be widely varied. However, even *in vitro* experiments are not free from unknown or uncontrolled influences. One reason why mathematical models become more and more a popular complementary tool to experiments is that they permit the study of hypotheses free from unknown or uncontrolled influences that occur in experiments. Many model types have been considered so far to model multicellular organization ranging from detailed individual-cell based models with explicit representations of the cell shape to cellular automata models with no representation of cell shape, and continuum models, which consider a local density averaged over many individual cells. However, how the different model description may be linked, and, how a description on a coarser level may be constructed based on the knowledge of the finer, microscopic level, is still largely unknown. Here, we consider the example of monolayer growth *in vitro* to illustrate how, in a multi-step process starting from a single-cell based off-lattice-model that subsumes the information on the sub-cellular scale by characteristic cell-biophysical and cell-kinetic properties, a cellular automaton may be constructed whose rules have been chosen based on the findings in the off-lattice model. Finally, we use the cellular automaton model as a starting point to construct a multivariate master equation from a compartment approach from which a continuum model can be derived by a systematic coarse-graining procedure. We find that the resulting continuum equation largely captures the growth behavior of the CA model. The development of our models is guided by experimental observations on growing monolayers.

*Keywords:* Tumor growth; monolayer growth; mathematical modeling; individual-based model; stochastic model; cellular automaton; coarse graining; multi-scale; master equation; Fisher–KPP equation.

### 1. Introduction

Despite spectacular progress in molecular biology, biochemistry and biophysics, qualitative and quantitative information on developmental processes, and processes on the maintenance and dysfunction of tissue is still sparse. One reason for this

is that multicellular organization involves complex processes on time scales ranging from  $\sim 10^{-9}$  s for molecular processes to  $\sim 10^7$  s for the development of an organism and length scales from  $10^{-9}$  m for a single molecule up to  $\sim 1$  m for an organism. It is neither possible nor desirable to take into account all details on all scales but rather to permit a distinction between relevant and less relevant processes on different scales. This concept is also pursued in medicine. For instance, melanoma which are essentially two-dimensional objects consisting of  $10^7$ – $10^8$  cells are historically characterized by their degree of asymmetry, their border irregularity, their color and their diameter (the ABCD's of melanoma). For a first diagnosis, this macroscopic information is believed to reflect the most essential information on the cellular and sub-cellular scales. In other sciences, such as material science [20], a distinction between relevant and less relevant scales is achieved by theoretical multiscale techniques and careful coarse graining methods which insure that only those microscopic properties are kept, which are relevant for the phenomenon on larger scales. Although the enormous complexity of biological systems makes the direct application of such techniques difficult, for selected situations rigorous techniques have been successfully applied. An example is the gliding and aggregation of bacteria in a chemoattractant field [69,70] for which limiting partial differential equations were rigorously derived from a stochastic equation of motion for each individual bacterium in a chemoattractant field generated by the bacterium. A similar link between microscopic and macroscopic equations has been suggested for interactive movement, aggregation and swarm dynamics of autonomous agents, such as birds by Alt *et al.* [1]. The type of macroscopic equations obtained in the latter case in which the autonomous agents attempt to find a balance between individual and collective behavior is reminiscent of the mechanisms that determine the macroscopic behavior of vehicles in traffic flow (e.g. Ref. 40, and references therein, and Refs. 41 and 42), or of pedestrians on trail systems [75]. Rigorous derivations of limiting PDEs for predator-prey systems have been given by Durrett and Levine [31] and, in a generalization of this method, by Cantrell and Cosner [13]. A rigorous *ansatz* to derive limiting PDEs for competing populations of cells has been pursued by Luckhaus and Triolo [54] and De Masi *et al.* [21]. They studied a birth-death model of two competing cell types, tumor and normal cells. In their approach, division of the tumor cells is not contact-inhibited while the normal cells can only divide if sufficient space is available. Both, tumor cells and normal cells are assumed to diffuse, the malignant ones faster than the healthy ones; the healthy ones moreover can hop only onto unoccupied lattice sites. In Ref. 54, they assumed stirring in order to obtain a continuum limit in a rigorous way, while in Ref. 21 this technically motivated assumption could be dropped. However, in the case where diffusion (or stirring), which is able to smooth out local spatial inhomogeneities in the cell density, does not exist (and a time scale separation is not possible), a rigorous coarse graining technique is still lacking. This is often the situation in *in vitro* growing cell populations. *In vitro* cell cultures are important experimental tools in understanding and analyzing the mechanisms involved in the growth of cell populations. As

opposed to *in vivo* systems, they can easily be manipulated (e.g. see Refs. 58 and 73) and hence permit systematic studies of the growth dynamics in growing cell populations, such as tumors. A commonly used experimental technique is the monolayer culture, where cells grow on a petri dish coated with specific proteins, such as extracellular matrix components, and with liquid media of specific compositions of e.g. nutrients and growth factors [5, 34]. Most tissue cells are not adapted to living in suspension and require anchorage to a solid surface to grow and divide (e.g. see Refs. 4 and 48). Consequently, most tissue cells stop proliferation when they have grown to a confluent monolayer [48, 53, 76]. This phenomenon is called “contact inhibition of growth,” or, “density limitation of growth.” Besides growth factors and cell-substrate adhesion, cell-cell adhesion [3, 53, 76], and apoptosis [72], selective programmed cell death triggered by a loss of cell-substrate contact, were found to be important factors of growth control. Some cancer cell-lines lack control mechanisms such as contact inhibition, anchorage-dependent proliferation and apoptosis, which enable them to grow to spheroidal aggregates (multicellular tumor spheroids) in suspension without any substrate contact [50, 65]. Treatment strategies for a number of diseases are often tested *in vitro* with respect to their efficiency and their toxicity before being applied to *in vivo* systems. This, in particular, includes testing drug, radiation and chemotherapy strategies against cancer.

However, even *in vitro* experiments are rarely free of unknown or uncontrolled influences. One reason why mathematical models are a useful tool in this field is that they do allow one to test hypotheses free from unknown or uncontrolled influences.

A number of mathematical models of growing tumor spheroids have been extensively studied so far. They may roughly be classified into (a) single-cell-based models and (b) continuum models. Single-cell-based models may be separated into three classes: (i) cellular automata models (CA) where each cell is represented by a single lattice site (e.g. see Refs. 24, 32 and 47; for a review, see Ref. 57); (ii) cellular automaton models where each cell is represented by many lattice sites [37, 43, 71]. This model type allows one to model complex cell shapes and to include physical mechanisms, such as cell-cell and cell-surface adhesion, and volume conservation, but it is difficult to directly relate experimental quantities on the cellular and sub-cellular scale to the model parameters; (iii) off-lattice models (for a review, see Ref. 25) where cells are either modeled as Voronoi polygons (e.g. Refs. 44 and 55), quasi-spherical particles that deform during cell division, (e.g. Refs. 26, 28 and 35), or deformable ellipsoids [61].

Among continuum models either kinetic approaches [7, 16, 77], or bio-mechanical approaches [12, 17, 46] have been studied so far. The former are based on reaction-diffusion type equations and free boundary problems in which each term is usually phenomenologically motivated. They do not include bio-mechanical effects such as the effect of stress on the tumor growth and shape, but allow one to easily include the detachment of cells. Bio-mechanical models so far decompose into two classes: firstly, models in which the outer proliferating layer of tumors is modeled as an elastic shell [16, 38]; secondly, approaches

that model tumors as two-phase fluids, one phase representing the tumor, the other phase the fluid medium around the tumor [18]. A systematic direct continuum approach that reflects the viscoelastic nature of the tumor in which the parameters on the macroscopic scale are extracted from the microscopic picture in a systematic way is still lacking. Furthermore, some models are hybrids combining a single cell-based description with a continuum description of molecules as glucose, oxygen or angiogenesis factors (e.g. Refs. 24 and 26).

Major advantages of CAs are that they are usually easier to implement and due to their simplicity run faster on computer, which is why they permit one to simulate large system sizes. Since CAs keep the individual-based picture, they are able to cover spatio-temporal fluctuations that may be important in the case of heterogeneous cell populations [2] or if cell death processes occur during treatment [22, 30]. Major disadvantages are that CAs are not primarily based on a direct physical representation of individual cells, which allows one to overlook certain physical effects. For example, apart from excluded volume considerations, bio-mechanical effects such as compressions or relaxations of cells and cell aggregates are hard to include. Off-lattice models naturally allow one to include smaller length scales and may be viewed as analogous to molecular simulations in statistical physics. However, their computing time requirement limits their usage to system sizes of at most  $\sim 10^5$ – $10^6$  cells, which corresponds to compact 3d-aggregates of  $\approx 1$ – $2$  mm in diameter. This is also much smaller than the typical size of a tumor at its clinical manifestation.

Continuous models can easily model significantly larger systems but how the equations and parameters have to be chosen in order to include the relevant information on the scale of individual cells is still largely unknown. A major advantage could result if one could combine the advantages of an off-lattice model to choose appropriate rules for a lattice model in such a way that the CA-approach represents all relevant features of the system behavior of the off-lattice approach and still maintains the individual-cell-based level. In this way, one could proceed to much larger system sizes and perform a sensitivity analysis over large parameter spaces which are largely valid for the off-lattice model as well. Both, the off-lattice model and the cellular automaton can serve as starting points for deriving a continuum theory. In this way, one obtains a hierarchy of description levels ranging from models that represent details on the subcellular scale up to models that subsume the subcellular and cellular scale in effective parameters.

In this paper, we illustrate how knowledge on the level of off-lattice models can be used to construct a CA which is then used as a starting point for deriving a continuous equation. Bru *et al.* [10] have performed experiments on *in vitro* cell cultures of different cell lines. These authors observed a linear expansion of the radius in monolayer cultures with cell-line dependent velocities of  $v = dR/dt = 1$ – $11 \mu\text{m}/\text{h}$ . Schifferer *et al.* [66] studied NIH3T3 cells which in culture initially form a sparsely distributed cell population (Hengstler, priv. communication). We use these results as a guide in this paper.

## 2. Model

### 2.1. Off-lattice-model

One way to set up a single cell-based model is to parameterize a cell and the interaction with other cells and the substrate by effective parameters or functions on the mesoscopic length scale that subsume the relevant microscopic (molecular) information. For example, although cells have a complex cytoskeleton network they essentially behave as a viscoelastic, or on short time scales, as an isotropic elastic body [3]. Their bio-mechanical properties therefore may be characterized by a very small number of material parameters, such as the modulus of elasticity and the Poisson number. These parameters are functions of characteristic quantities on the molecular scale and may be actively regulated by the cell [4]. The spatio-temporal averaged effect of the molecular processes that are involved in both the formation and the release of bonds between cell adhesion molecules anchored in the cell membrane (macroscopically manifested as adhesive cell–cell contacts) and the reorganization of the cytoskeleton that accompanies the deformation of an originally spherical cell during the formation of a cell–cell or a cell–substrate contact may be represented by an appropriate functional form of an interaction energy between cells.

While isolated cells in cultures or suspensions often have a spherical shape, in dense monolayers they often adopt a polygonal (or cuboid-like) shape. In the cell cycle, cells often deform before they divide. The model assumes that each cell is spherical directly after cell division and deforms into a dumb-bell during the cell cycle, i.e. actively changes its “equilibrium shape” (Fig. 1(a)). A cell, however, can grow only if it is not significantly compressed or deformed. We assume that a cell stops growing at a certain degree of deformation or compression. We varied the deformation threshold at which this growth stop occurs between 10–25% of the cell diameter immediately after cell division (Fig. 1(a)). We assume that if the deformation falls below the threshold again, the cell can re-enter the cell cycle and continue growing. Often in cell cultures, apoptosis of cells is observed. In monolayers, this occurs in particular in the interior. However, as shown elsewhere [26], apoptosis in the monolayer interior has no effect on the growth kinetics of monolayers, which is why we do not consider apoptosis in this paper. The combination of attractive and repulsive interactions between cells  $i$  and  $j$  may be approximated by the interaction energy:

$$V_{ij} = V_{ij}^{\text{attr}} + V_{ij}^{\text{rep}}, \quad (1)$$

where  $V_{ij}^{\text{attr}} = -\varrho A_{ij} V_{\text{smol}}$  is the adhesion energy.  $\varrho$  is the surface density of adhesion molecules,  $A_{ij}$  the contact area between cells  $i$  and  $j$  and  $V_{\text{smol}}$  the energy of a single bond between adhesive cell receptor molecules. The repulsive contribution  $V_{ij}^{\text{rep}}$  has been calculated by the the Hertz-model of two homogeneous elastic spheres [35, 51]:

$$V_{ij}^{\text{rep}} = (2\tilde{R} - d_{ij})^{5/2} \frac{2}{5\tilde{E}} \sqrt{\frac{\tilde{R}}{2}}. \quad (2)$$

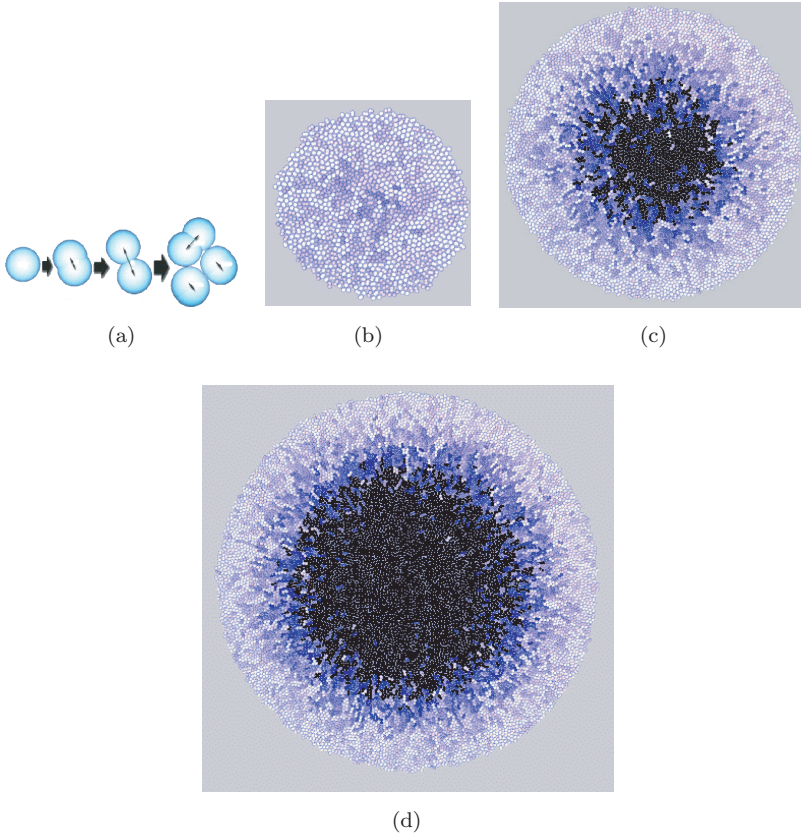


Fig. 1. Typical simulation scenario in the off-lattice model starting from (a) a single cell to three cells and aggregates of (b)  $N = 100$ , (c)  $N = 1,000$ , and (d)  $N = 10,000$  cells. (Further technical details are given elsewhere [26].) The radius of the circles that belong to a dumb-bell is  $\tilde{R}$  (a cell immediately after division is spherical with radius  $\tilde{R}$ ). The lighter the shading, the larger the proliferative activity. At  $N \geq 1,000$  cell proliferation is confined to a boundary layer.

Here,  $\tilde{R}$  is the cell radius (see Fig. 1):

$$\tilde{E} = \frac{3}{2} \left( \frac{1 - \sigma^2}{E} \right), \quad (3)$$

with  $\sigma$  being the Poisson ratio and  $E$  the modulus of elasticity. Then, the interaction area  $A_{ij} = \pi(2\tilde{R} - d_{ij})\tilde{R}/2$  results immediately from the Hertz model [51]. The results of the simulations are very robust against the precise shape of the interaction potential. For an equivalent choice of parameters the results on expanding monolayers are even quantitatively very similar and depend only slightly on whether one uses a harmonic-like interaction energy (linear, reversible springs), an interaction energy according to the Hertz model [35, 51] or according to the JKR-model [26]. All approximations for the interaction energy assume that cells are isotropic elastic bodies. The harmonic-like interaction energy assumes cuboid-shaped cells, the Hertz

model spherical cells in a limit where cell adhesion is a consequence of deformation and the JKR-model assumes spherical cells in a limit where the cell–cell-adhesion causes cell deformation. However, the JKR-model also takes into account the stretching of adhering cells if they are pulled apart, which leads to a hysteresis effect.

Beysens *et al.* [8] have illustrated experimentally that cells may be considered similar to particles in a fluid. For example, cells in culture medium and embryonic cells in cell aggregates have been observed to perform a random diffusion-like motion. Although the motion is mainly the consequence of an active migration process, it may be approximated on the mesoscopic scale by an effective diffusion-like process.

### 2.1.1. Monte-Carlo method

Figure 1 shows a Monte-Carlo simulation based on the Metropolis algorithm using the Hertz model (model simulations using the JKR model can be found in Ref. 26). Such a simulation corresponds to solving a master equation for the temporal development of the multivariate probability distribution function  $p((\underline{x}_1, \underline{a}_1), (\underline{x}_2, \underline{a}_2), \dots; t; N)$ , where  $\underline{x}_i$  is the position,  $\underline{a}_i$  denotes the dumb-bell axis of cell  $i = 1, 2, \dots, N$  (Fig. 1).  $t$  denotes time;  $N$  the population size. The idea is to change a configuration of cells by moves (translations, rotations, growth steps, division) and assess the moves using the Metropolis algorithm. A move is accepted with probability  $p = \min[1, \exp(-\Delta V/F_T)]$ , where  $V = \sum_{i < j} V_{ij}$  is the total interaction energy of the multicellular configuration,  $\Delta V$  the energy change that would result from the move.  $F_T$  is a parameter which measures the activity of a cell and may be interpreted as a formal equivalent to  $k_B T$  in fluid systems ( $k_B$ : Boltzmann constant,  $T$ : temperature). Note that  $F_T$  reflects the ability of cells to actively explore their environment and is not a consequence of collisions of cells with smaller fluid particles. The Monte-Carlo dynamics models the development of cell populations in configuration space,  $t$  is time and  $N$  the population size. As already pointed out above, the dynamics modeled in this way corresponds to a master equation, which is a linear integro-differential equation.

### 2.1.2. Langevin equations

By expanding the master equation for small step sizes (migration steps, orientation angles and growth steps), one can obtain the equivalent Fokker–Planck-equation, which is a partial differential equation for the probability density of the cell configuration. The Fokker–Planck equation can generally be shown to correspond to systems of stochastic differential equations. The stochastic differential equations are the equations of motion for the individual cells [35]. The numerical integration of the equations of motion corresponds to tracking single realizations of the stochastic process of cell migration, orientation changes and growth. We circumvent this lengthy procedure here and instead directly write down the model formulation

in terms of stochastic differential equations. The approach based on equations of motion often permits an interpretation on a more intuitive basis since the effect of forces on the cells, of friction or fluctuation can be seen more directly, which is why we use it here to interpret the simulation results. Note, however, that the approaches are statistically equivalent.

The equation of motion for the translation of an individual cell  $i$  can be approximated by a Langevin-equation of the general type

$$\begin{aligned}
 & \underbrace{M_i \frac{d\mathbf{v}_i}{dt}}_{(0)} + \underbrace{\underline{\underline{\Gamma}}_{cs}^f \frac{A_i^{cs}}{A_i} \mathbf{v}_i}_{(1)} + \sum_{j \text{ nm } i} \underbrace{\underline{\underline{\Gamma}}_{cc}^f \frac{A_{ij}}{A_i} (\mathbf{v}_i^{ij} - \mathbf{v}_j^{ij})}_{(2)} \\
 & = \underbrace{\int_0^t K_m(t-t') \mathbf{v}(t') dt'}_{(3)} + \underbrace{\sum_j \mathbf{F}_{ij}}_{(4)} + \underbrace{\mathbf{f}_i(t)}_{(5)}. \tag{4}
 \end{aligned}$$

Here,  $\mathbf{v}_i = \frac{d\mathbf{r}_i}{dt}$  denotes the velocity of the cell at time  $t$ ,  $\mathbf{r}_i$  its position,  $\mathbf{F}_{ij}$  the force from cell  $j$  on cell  $i$ .  $M_i$  is the mass of cell  $i$ .  $\mathbf{v}_i^{ij} = \mathbf{v}_i + \underline{\underline{\Omega}}_i \times \mathbf{r}_i^{ij}$  denotes the velocity of cell  $i$  at the contact point between cells  $i$  and  $j$ ,  $\mathbf{r}_i^{ij}$  the vector from the center of mass of cell  $i$  to the contact area between cells  $i$  and  $j$ .  $\underline{\underline{\Gamma}}_{cs}^f$  and  $\underline{\underline{\Gamma}}_{cc}^f$  are tensors and denote the cell–substrate and cell–cell friction, respectively.  $\underline{\underline{\Gamma}}_{cs}^f$  depends on whether the substrate is homogeneous or inhomogeneous as well as on the cell geometry and polarity. If, for example, the cell is dividing and has a dumb-bell shape, and the environment is homogeneous and isotropic,

$$\underline{\underline{\Gamma}}_{cs}^f = \gamma_{\parallel}^{cs} \hat{\mathbf{b}}\hat{\mathbf{b}} + \gamma_{\perp}^{cs} [\underline{\underline{\hat{I}}} - \hat{\mathbf{b}}\hat{\mathbf{b}}].$$

The unit vector  $\hat{\mathbf{b}}$  points into the direction of the cell axis (i.e. here:  $\hat{\mathbf{b}} = \hat{\mathbf{a}}$ ).  $\underline{\underline{\hat{I}}}$  is a unit tensor.  $\hat{\mathbf{b}}\hat{\mathbf{b}}$  is a tensor product.  $\hat{\mathbf{b}}\hat{\mathbf{b}}\mathbf{v}_i$  is the velocity parallel,  $[\underline{\underline{\hat{I}}} - \hat{\mathbf{b}}\hat{\mathbf{b}}]\mathbf{v}_i$  the velocity perpendicular to the axis of the cell.  $\gamma_{\parallel}^{cs}$  and  $\gamma_{\perp}^{cs}$  are friction coefficients that quantify the friction parallel and perpendicular to the axis. If the cell is spherical and the environment is homogeneous and isotropic,  $\underline{\underline{\Gamma}}_{cs}^f = \gamma \underline{\underline{\hat{I}}}$  (see Appendix A).

(0) denotes the inertia term and can be neglected in cell movement where friction dominates inertia due to large cell-environmental friction (limit of small Reynold numbers [60]). (1) denotes the friction-term of a cell with its surrounding medium (substrate, suspension), (2) the friction term of a cell  $i$  with its neighbor cells  $j$ , (3) a memory term that accounts for the persistence that is often observed during cell motion.  $K_m(t-t')$  is a memory kernel. (4) denotes the forces on cell  $i$  exerted by its neighbor cells  $j$ , (5) the (active) random movement of cells. We assume that all memory affects are absorbed in term (3) and the noise  $\mathbf{f}^i(t)$  is uncorrelated such that, for the autocorrelation function,

$$\langle \mathbf{f}(t) \mathbf{f}(t') \rangle = 2 \underline{\underline{\hat{I}}} \delta(t' - t), \tag{5}$$

holds. Further, we assume  $\langle \mathbf{f}(t) \rangle = 0$ .  $\underline{\underline{\hat{I}}}$  quantifies the amplitude of the autocorrelation function. In the case of isotropic friction and spherical cells, only the diagonal elements of the tensor are different from zero and all have the value  $\gamma^2 D$ ; hence

$\hat{\underline{\Gamma}} = 2\gamma^2 D \hat{\underline{\Gamma}}$  ( $D$  the cell diffusion constant).  $A_i$  is the cell surface area of cell  $i$ ,  $A_{ij}$  the contact area between cells  $i$  and  $j$ ,  $A_i^{cs}$  the contact area between cell  $i$  and the substrate.  $\underline{\Omega}$  is the angular velocity and takes into account that a cell may change orientation. (For non-spherical cell shapes, such as during mitosis and for polar cells, an equation of motion for the angular velocity has to be considered.) On time scales large compared to the memory of the cell, the memory term (3) can be neglected. This is assumed here. In the case of monolayer growth, all cells perform an almost radial movement with approximately equal velocity,  $\underline{v}_i \approx \underline{v}_j$ , for neighboring cells  $i$  and  $j$ .

Rescaling the noise by  $\underline{f}^i(t) = \sqrt{2\gamma^2 D} \underline{\eta}^i$  yields

$$\frac{d\underline{r}_i}{dt} = \frac{1}{\gamma} \sum_{j=1}^N \underline{F}_{ij} + \sqrt{2D} \underline{\eta}^i(t), \quad (6)$$

where  $\langle \eta_m^i(t) \eta_n^j(t') \rangle = \delta_{ij} \delta_{mn} \delta(t-t')$  (in the case of large forces, the noise term may be omitted [29]).  $m, n = 1, 2, 3$  denote the components of the vector  $\underline{\eta}^i$ ,  $i, j$  cells  $i$  and  $j$ . In this form of the equation, the parameter dependencies become directly obvious. Friction reduces the effect of the forces on cell  $i$  while an increase of the diffusion rate  $D$  increases the effect of the random migration. Beysens *et al.* [8] suggested to link the diffusion constant  $D$  and the friction coefficient  $\gamma$  by an effective Einstein-relation  $D = F_T/\gamma$ , where  $F_T$  replaces  $k_B T$  in the equivalent equation for fluid particles. Thereby,  $F_T$  can be calculated from the friction coefficient and the diffusion constant which links the Monte-Carlo method to the Langevin method. We use the cell diameter  $l$  as a reference length scale, the intrinsic cell cycle time  $\tau$  as a reference time scale, and  $F_T$  as a reference energy scale. As in the MC-simulation, growth is modeled by a deformation of the cell into a dumb-bell by small stochastic increments of size  $\ll \tilde{R}$  (Fig. 1(a)). In this case, cells adopt a dumb-bell shape and hence orientation changes have to be taken into account, which are partly driven by active orientation changes and partly by a torque. In the overdamped case and in the absence of memory effects, the equation for the angular momentum can be written as (Appendix A):

$$\underline{\hat{\Gamma}}_i^{cs} \underline{\Omega}_i = -\underline{\hat{\Gamma}}_i^{cc} \sum_j \underline{\hat{\Gamma}}_i^{ij} \times (\underline{v}_j^{ij} - \underline{v}_i^{ij}) + \frac{a_i}{2} \hat{\underline{a}}_i \times (\underline{F}_i^{(1)} - \underline{F}_i^{(2)}) + \hat{\underline{\Gamma}}_i^\xi. \quad (7)$$

Here, it is assumed that the mass of the cells is concentrated in the spheres of the dumb-bell (with axis length  $a_i$  and axis orientation  $\hat{\underline{a}}_i$ ). The term on the left-hand side denotes the friction of cell  $i$  with the substrate, the first term on the right-hand side the cell-cell friction, the second term the external torque on the cell (where we assumed for simplicity that the forces  $\underline{F}_i^{(1)}$ ,  $\underline{F}_i^{(2)}$  act on the centers of the circles 1, 2 that belong to the dumb-bell  $i$ ), and the third term an external torque.  $\hat{\underline{\Gamma}}_i^\xi$  is the fluctuating torque with  $\langle \hat{\underline{\Gamma}}_i^\xi(t) \rangle = \underline{0}$  and autocorrelation

$$\langle \hat{\underline{\Gamma}}_i^\xi(t) \hat{\underline{\Gamma}}_i^\xi(t') \rangle = \underline{\underline{G}}_i \delta(t-t') \quad (8)$$

in the case where correlations are neglected. Here,  $\underline{\underline{G}}_i$  is a matrix and mimics the amplitude of the random component of the cell orientation changes. For colloidal

particles,  $\underline{G}_r$  is related to the friction matrix [22], while for cells it is controlled by the cell itself.

In summary, the cell shape has been parametrized by its diameter and the degree of its deformation (during cell division), the cell material properties by the (Young) modulus of elasticity, the cell kinetics by the cycle time, the cell migration behavior by a stochastic equation of motion (where the noise autocorrelation amplitude is determined by the cell diffusion constant), and the cell–cell interaction by an interaction potential energy. Since all model parameters can be expressed in terms of measurable quantities, they can all in principle be determined by experiments. Figure 1 shows a typical simulation scenario, Fig. 2 the temporal development of the monolayer radius for different friction coefficients  $\gamma$  and diffusion constants  $D$ . For all parameter choices, the qualitative growth kinetics is the same: the tumor initially grows exponentially fast ( $N = e^{t/\tau_e}$ ,  $\tau_e$  is the effective cycle time and defined in Fig. 2) then crossing over to a linear expansion of the monolayer radius. The crossover time depends on the model parameters. Note that the expansion velocities  $v$  lie within the range observed by Bru [10]. Varying  $D$  for a given  $F_T$  corresponds to varying  $\gamma$  since both can be linked by  $D = F_T/\gamma$ . A smaller  $\gamma$  results in a larger expansion velocity. The linear expansion is a consequence of a confinement of cell proliferation to a small surface layer. Interior cells experience a deformation too large to be capable of further growth and division, which is why they do not contribute to the expansion of the monolayer. The expansion velocity

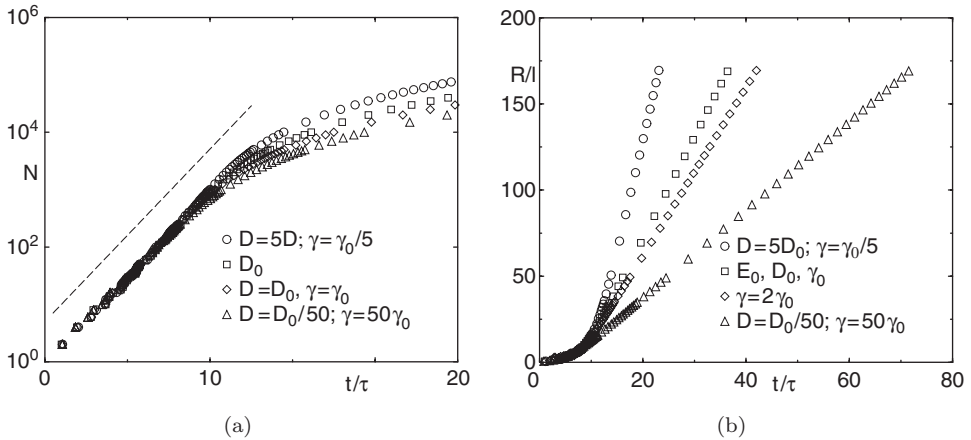


Fig. 2. Growth kinetics of cell aggregates in off-lattice model. (a) Population size  $N$  versus  $t$  in a semilogarithmic plot. ( $D_0 = 4.6 \mu\text{m}^2/\text{h}$ ,  $\gamma_0 \approx 0.1 \text{Ns/m}$ ,  $E_0 = 450 \text{Pa}$ ,  $l = 10 \mu\text{m}$ ,  $\tau = 19 \text{h}$ .) The symbols denote simulation results, the dashed line  $N = N_0 e^{t/\tau_e}$ .  $\tau_e$  was taken from a fit to the exponential regime of Fig. 2(a). The intrinsic cycle time  $\tau$  is defined as the average cycle time of an isolated cell. (b) Plot of the monolayer radius  $R$ . We have varied the diffusion constant  $D$  and the friction coefficient ( $\gamma$ ) to test the parameter sensitivity of the expansion velocity of the multicellular aggregate. (The parameters were estimated from the experimental literature.)

is determined by the size of the proliferating layer. A decrease of  $\gamma$ , or an increase of  $D$  in combination with a decrease of  $\gamma$  relaxes stress at the monolayer boundary and therefore increases  $v$ . Also, other properties on the cellular scale such as the biomechanical properties of a cell or the trigger for growth stop may be able to influence the expansion velocity  $v$ . Hence,  $v = v(\gamma, D, \dots)$  becomes a function of properties of cells and their environment on a sub-cellular level.

A major limitation of the off-lattice model is its large computing time requirement. Simulations up to a cell population size of  $N \sim 10^5$  cells take up to 2 weeks on a Pentium IV-3GHz processor.

Some cell lines such as NIH3T3-HER2 cells initially form a sparse distribution (Fig. 3). As we will show below, this can be explained by assuming no adhesion between the cells and a fast cell movement (modeled by a large  $D$ ). In this case, a systematic parameter sensitivity analysis by the off-lattice model is not feasible. Hence, if either (i) the system size becomes large or (ii) cell-cell adhesion is negligible ( $V_{ij}^{\text{adh}} \approx 0$ ) and  $D$  is large, then alternative model approaches are needed for a systematic study of the system behavior. Hence, for a systematic study of sparsely distributed systems and generally for large systems alternative approaches

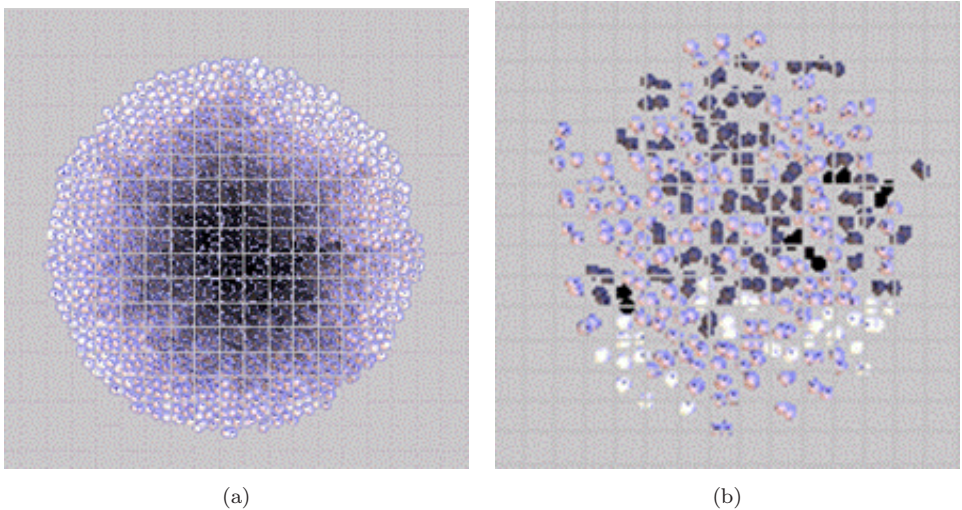


Fig. 3. Generation number for (a) large adhesion and (b) no adhesion in simulated monolayers. Light cells have performed more cell divisions than dark cells. The left picture shows a clear tendency. Light cells are located at the tumor boundary, while dark cells are in the tumor interior. This indicates that the transition to the surface-growth regime in which the tumor diameter expands as  $L \propto t$  has already occurred. The cell population in the right picture shows no systematic spatial generation pattern, i.e. whether a cell divides or not depends on the cycle time distribution only (the division of the cells are independent stochastic processes), not on the spatial position of the cell in the cell population. Different from exponentially fast growing cell populations in compact aggregates where the monolayer diameter also grows exponentially fast, the tumor diameter in the right picture expands as  $L \propto \sqrt{t}$  since pushing of cells does not occur.

are needed. If the advantages of single-cell-based models should still be maintained, simpler models of individual cells have to be used which, however, should capture the system behavior found by the off-lattice model. A potential approach along this line is to establish a cellular automaton model with a proper choice of rules.

### 3. Cellular Automaton

Eden [32] suggested a model of avascular tumor growth on a square lattice, where each lattice point can at most be occupied by a single cell. This assumption takes into account the excluded volume effect: each cell occupies a particular volume in space which cannot be occupied by another cell at the same time. Different versions of the Eden model have been suggested, distinguished by the way cells are selected for division (see e.g. Ref. 49 and references therein). In each of these versions, a cell division can only take place onto an unoccupied lattice site adjacent to an occupied lattice site. In the William–Bjerkness model [78] for tumor growth, a pair of neighbor sites, one being occupied and one being free, has a probability of  $\alpha$  to become both occupied and of  $\beta$  to become both unoccupied in the next instant of time. For  $\alpha/\beta > 1$ , an existing cluster grows. In the Richardson model [64], each free site adjacent to an occupied site becomes occupied with probability  $p$  (independent for each free site). For  $p = 1$ , the growth process is completely deterministic; for  $p \rightarrow 0$  combined with an appropriate rescaling of time, the Eden model is recovered. Large Eden clusters contain growth sites only in a thin surface layer which occupies a negligible fraction of the cluster volume in the limit  $N \rightarrow \infty$ . This implies that the clusters attain a compact shape as they become larger (e.g. Refs. 49 and 64). Richardson argued that the standard Eden model in this limit approaches a perfect sphere. Bramson and Griffeath [9] have shown that the William–Bjerkness model asymptotically approaches a ball of linearly-in-time expanding radius. Batchelor and Henry [6] have looked at the cluster symmetry in the Eden model and a noise-reduced variant. This corresponds to the F-family models by Richardson [64]. They assigned a counter  $M$  to each cell and increased it by one each time the cell was selected. After having selected a cell  $m$  times, it was divided according to the rules of the standard Eden model. The case  $m = 1$  then is the original Eden model. Batchelor and Henry found in computer simulations in  $d = 2$  that (i) the border of the Eden cluster becomes much smoother as  $m \rightarrow \infty$ , (ii) the Eden cluster approaches a diamond shape the quicker  $m$  grows (Fig. 4). However, all of these models assumed that only cells at the tumor border were able to divide. The expansion velocity of the monolayer in this case is  $v \approx l/\tau_e$ , where  $l$  is the cell diameter and  $\tau_e$  the effective cycle time, which is defined in Fig. 2. Typical cell diameters range from  $\sim 8\text{--}18\ \mu\text{m}$ , typical cycle times from  $\sim 12\text{--}36\ \text{h}$ , so  $v < 1.5\ \mu\text{m/s}$ , which is incompatible with the experimental observations in most monolayers and tumors [10]. However, the proliferating layer in the off-lattice model was larger than one cell diameter (Figs. 1 and 2). This suggests the introduction of the number of cells  $k$  that a dividing cell is able to push aside or to stimulate to actively migrate away

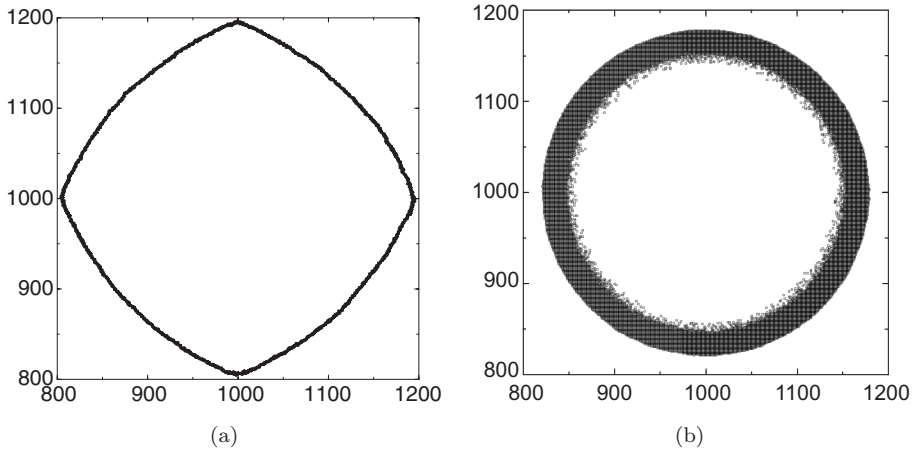


Fig. 4. (a) The morphology of the noise-reduced variant of the classical Eden model has a diamond shape. Here, a cell has to be chosen  $m$ -times until it divides. (b) If a dividing cell is able to push at most  $k$  other cells aside, or, to stimulate at most  $k$  neighbor cells to migrate aside in order to provide free space for division, the morphology approaches an almost circular shape. The black area denote cells in the cell cycle. The classical model (a) is a special case of the model (b). In (a)  $m = 60$ ,  $k = 0$ , in (b)  $m = 60$ ,  $k = 22$ ; in (a) and (b),  $N = 100,000$ .

as an additional parameter. Thereby parameter  $k$  expresses the effect of the forces (or stimuli) in the off-lattice model.

Our model algorithm can be subsumed by the following rules (all length units are expressed in multiples of the cell size  $l$ ; all time units are expressed in multiples of the intrinsic cycle time  $\tau$ ):

- R1 Each lattice site can be occupied by at most one single cell. This takes into account that a lattice site can be occupied by only one cell at the same time.
- R2 A dividing cell is able to push aside at most  $k$  neighbor cells. We pursue this by assuming that a cell can divide if and only if there is at least one free neighbor site within a circle of radius  $\Delta R = k + 1$  around the dividing cell. The pushing process should not be performed only along the axes of the lattice since this enforces artifacts by the square lattice symmetry.
- R3 When a cell divides, one of its daughter cells is placed at the original position of the mother cell, the other daughter cell is placed next to it and the local cell configuration is shifted and re-arranged along the line that connects the mother cell with the closed free lattice site within a circle of radius  $\Delta R$  in such a way that this closest free lattice site is now occupied by a cell. This algorithm mimics a realistic re-arrangement process that may occur as a consequence of mechanical stress exerted by a growing cell on its neighbor cells as is observed in the off-lattice model. (The second daughter cell could also be directly placed on the closest free lattice site within a circle of radius  $\Delta R$ .)

This, however, leads to the same spatial pattern only as long as all cells have identical properties as is the case in this article.)

- R4 The (intrinsic) cell cycle time  $\tau'$  is distributed due to a Erlang-distribution, the discrete analog of the  $\Gamma$ -distribution, i.e.

$$f(\tau') = \lambda_m \frac{(\lambda_m \tau')^{m-1}}{(m-1)!} \exp\{-\lambda_m \tau'\} \quad (9)$$

with  $\lambda_m = m$  such that  $\langle \tau' \rangle = \tau = 1$ . For  $m = 1$ ,  $f(\tau)$  is Poisson-distributed. For  $m \rightarrow \infty$ ,  $f(\tau')$  approaches a  $\delta$ -distribution, peaked at  $\tau' = \tau$ .

- R5(a) A cell hops with rate  $\phi$  to a free neighbor site irrespective of the number of neighbor cells before and after its hop. This rule corresponds to the limit of no cell–cell adhesion.
- R5(b) A cell hops with rate  $\phi$  to a free neighbor site if by this move the number of its free neighbor sites does not increase. We compare two hopping rules: (i) hopping to one of the four possible neighbor sites in horizontal and vertical direction, and (ii) hopping to one of the eight possible neighbor sites in horizontal, vertical, and diagonal directions. This rule corresponds to the limit of strong cell–cell adhesion. The rule insures that de-attachment of cells from the expanding cluster does not occur and generates cell movement along the monolayer surface if  $\phi > 0$ . At the same time, it accounts for the random movement of isolated cells, for example, the precursor cell of a monoclonal, or isolated cells that would emerge if as a consequence of a death process (e.g. the effect of a therapy) the neighbor cells of a cell were eliminated.

The waiting time  $\tau_\phi$  between two hops is distributed due to a Poissonian:

$$f(\phi) = \phi \exp\{-\phi \tau_\phi\} \quad (10)$$

Note that unlike the rules R5(b)(i) and (ii), the probability of a cell to move in the off-lattice model depends on the potential energy change. The total change of the potential energy depends on the change of the number of neighbor cells of a cell. The rule used here neglects this influence. It could be taken into account by choosing the transition rates in the CA model as  $\propto e^{-\Delta V_{ij}/F_T}$  with  $V_{ij} \propto \#(NNs)$ . However, this assumption slows down the simulations considerably and would, for strong cell–cell adhesion forces, only slightly modify the cell migration along the monolayer surface. (It favors configurations in which each cell has a maximum number of neighbors.)

### 3.1. *Limit of no free hopping*

We in this subsection, consider a regular square lattice and a Dirichlet lattice. In the next subsection, where we study the case of freely hopping cells, we consider a regular lattice only.

### 3.1.1. Regular square lattice

If cell–cell adhesion is strong, cells do not de-attach from the main cluster and rules R5(b)(i) and (ii) apply.  $\phi > 0$  generates cell movement along the monolayer surface. This may have consequences for the “critical behavior” of the surface in terms of the roughness, growth, and dynamic exponent (see e.g. Refs. 25, 39 and 49) that have recently been used to characterize the surface growth dynamics of expanding tumors [10]. In particular,  $\phi = 0$  is believed to correspond to the so-called KPZ-universality class that has been found for the Eden model (e.g. Refs. 39 and 49) while  $\phi \gg \lambda$  may generate an “MBE-like” behavior at least within a transient regime. However, here we focus on the expansion kinetics which from our simulations does not show detectable differences for realistic ranges of  $\phi$ , which justifies the setting of  $\phi = 0$ .

We perform simulations for  $m = 1$  (Poissonian distributed (intrinsic) cycle time) and  $m = 60$  (as an example of a sharply peaked cycle time distribution at  $\tau$ ). Figure 4 shows the monolayer geometry in the CA-simulation for  $m = 60$ ,  $k = 0, 22$ ; Fig. 5 shows the monolayer geometry for  $m = 1$  and  $k = 3, 22$ . The result for  $k = 0$  and  $m = 60$  shows lattice anisotropies which are known as noise-reduction effects (Fig. 4). At large  $k \gg 0$ , these lattice anisotropies, however, almost disappear. The figures suggest that in both limits,  $k \rightarrow \infty$  as well as  $m \rightarrow 1$ , the cluster-geometry adopts a circular shape. (The latter result has been proved by Richardson [64].)

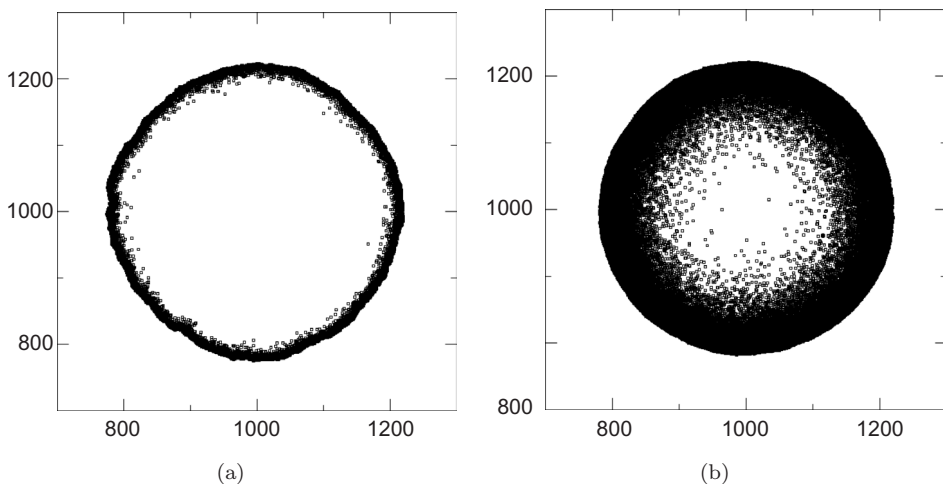


Fig. 5. Effect of cycle time distribution and of  $k = \Delta R - 1$  on the monolayer. Different from Fig. 4, the cycle time is Poissonian distributed ( $m = 1$ ). (a)  $k = 3$ , (b)  $k = 22$ . The black dots denote the active sites. For larger  $k$ , the thickness of the proliferating rim is larger and the surface of the monolayer smoother. Furthermore, a comparison with Fig. 2(b) shows that the proliferating layer (black area) for a given value of  $k$  is larger for the Poissonian distributed cycle times than for the sharp cycle time distribution obtained for large  $m$ . This is also reflected in the growth kinetics, where one roughly finds  $v \approx \Delta R/\tau$  for Poissonian-distributed cycle times, and  $v \approx \ln(2)\Delta R/\tau$  for  $\delta$ -distributed cycle times (Fig. 7). In (a) and (b),  $N = 100,000$ .

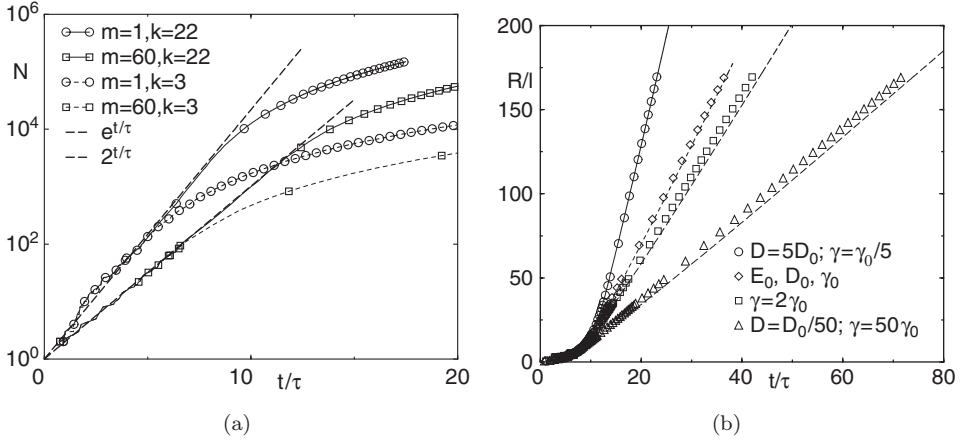


Fig. 6. (a) Effect of the parameter  $m$  on the initial growth phase of the monolayer population  $N$ . The observed, effective cycle time  $\tau_e$  in the exponential regime is given by a fit to the function  $N = N_0 e^{t/\tau_e}$ . For  $m = 1$ ,  $\tau_e = \tau$  while for  $m = 60$ ,  $\tau_e \approx \tau/\ln(2)$ , hence  $N = N_0 e^{t/\tau_e} \approx N_0 2^{t/\tau}$ . Hence, for a sharply peaked cycle time distribution (large  $m$ ), the growth of the population is slower than for a broad cycle time distribution (small  $m$ ) even if the intrinsic cycle time  $\tau$  is the same. (b) Comparison of growth kinetics of monolayer radius between off-lattice model and lattice model. The symbols denote the off-lattice simulations. The lines denote the lattice simulations with  $m = 60$ . The curve for  $D = 5D_0$ ,  $\gamma = \gamma_0/5$  corresponds to  $k = 22$ , for  $E_0, D_0, \gamma_0$  to  $k = 9$ , for  $\gamma = 2\gamma_0$  to  $k = 7$ , and for  $D = D_0/50$ ,  $\gamma = 50\gamma_0$  to  $k = 3$ .

Figure 6 shows that as in the off-lattice simulations, the population size  $N(t)$  initially increases exponentially fast (Fig. 6(a)), crossing over to a linear expansion of the monolayer radius at large times (Fig. 6(b)). However, for the same intrinsic cycle time  $\tau$ , the population grows faster for small  $m$  than for large  $m$ , i.e. if the cycle time distribution  $f(\tau)$  is broad, the population grows faster. The reason is that if the cycle time distribution is broad, those cells with the shortest cycle time divide the fastest. Among their daughter cells, again those cells with the shortest cycle time divide the fastest such that the observed (effective) cycle time is determined by the fastest dividing cells and hence smaller than  $\tau$ . In case the cycle time distribution is sharply peaked, such a cascade-like division cannot occur and all cells divide with almost the same cycle time (at  $m \rightarrow \infty$ , cell division becomes synchronized). Figure 6(b) shows a comparison between the growth curves for the monolayer diameter  $L$  obtained in the CA-model with  $m = 60$ , and those obtained in the off-lattice model. The results of the off-lattice approach can be modeled by tuning the parameter  $k = \Delta R - 1$ . The biophysical and kinetic small scale parameters in the off-lattice model control  $v$  by controlling the size of the proliferating rim, i.e.  $\Delta R = \Delta R(E, D, \tau, l, \dots)$ . Hence, the essential information which allows one to model the range of growth velocities observed in the experiment can be subsumed in the simple parameter  $k = \Delta R - 1$ .

The parameters  $k$ ,  $m$  and  $\phi$  can be obtained as follows:

- Cycle time distribution (parameter  $m$ ): Assume the intrinsic cycle time  $\tau$  is known. Then,  $m$  results from a fit of  $N \propto e^{t/\tau_e}$  to the initial exponential growth regime in the off-lattice simulation. Here,  $\tau_e$  is the observed cycle time in the experiment. In the case where  $m = 1$ ,  $\tau_e = \tau$  while for  $m \rightarrow \infty$ ,  $\tau_e \rightarrow \tau/\ln(2)$ .  $m$  controls dispersion of the cycle time distribution, which affects the growth of the total cell populations size. As shown below (Sec. 4.1)  $\tau_e^{-1} = \tau^{-1}((2^{1/m} - 1)m)$ . This permits one to conclude  $m$ . In our off-lattice simulations, the cycle time distribution was sharply peaked at  $\tau$ , which is why we have chosen a large  $m$  in our CA simulations for Fig. 6(b).
- $k (= \Delta R - 1)$ : The crossover from exponential to linear monolayer expansion occurs if the size of the expanding monolayer becomes larger than twice the size of the proliferating rim, i.e. at  $L_{cr} = 2\Delta R$  with  $L_{cr} = 2R_{cr}$ . For  $R \leq R_{cr}$ , all cells are able to divide hence the growth is exponentially fast. As shown in Fig. 7(a), the growth velocity in the linear expansion regime is  $v \approx \Delta R/\tau_e$  (in un-scaled units). Note that  $k = \Delta R - 1$  not only controls the expansion velocity  $v$  in the linear regime but also the length of the initial exponential growth regime (Fig. 6(a)). In order to determine  $\Delta R$ , one can thus run the off-lattice simulation until this crossover point and determine  $\Delta R$  from  $L_{cr} = 2\Delta R$ .
- Hopping rate  $\phi$ : The hopping rate  $\phi$  can be obtained from the random movement of an isolated cell, for example, using  $D = l^2\phi/2d$  for rule R5(b)(i) or rule R5(a), where  $d$  is the spatial dimension (here,  $d = 2$ ).

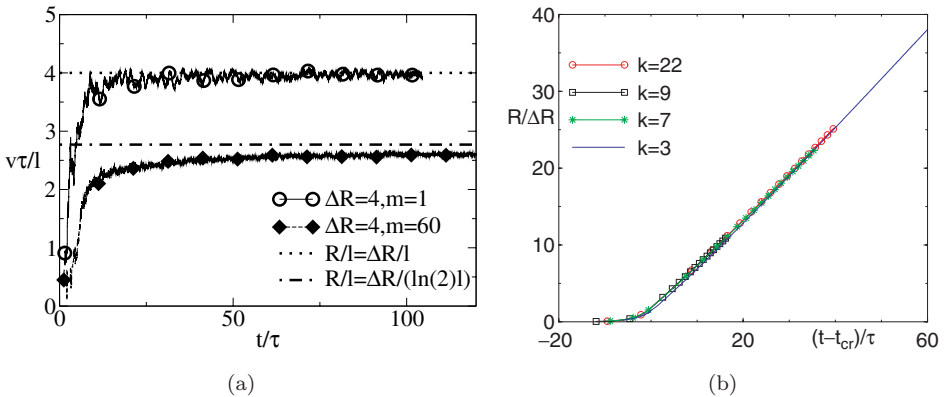


Fig. 7. (a) Growth velocity  $v = dR/dt$  in the linear expansion regime (in scaled units) for  $\tau_e = \tau$  (for  $m = 1$ ) and  $\tau_e = \tau/\ln(2)$  (for  $m = 60$ ) at  $k = 3$ . The curves were obtained by numerical differentiation of  $R(t)$ . The growth velocity is  $v \approx \Delta R/\tau_e$  ( $\Delta R = k + 1$ ). (b) If the axes rescaled due to  $R/l \rightarrow R/\Delta R$ , and  $t/\tau \rightarrow (t - t_{cr})/\tau$  (for details, see text), a collapse of the curves from Fig. 6(b) for different  $k = \Delta R - 1$  is obtained (shown for  $m = 60$ ). The slope is  $\approx 0.64$ . Since the slope is still slightly increasing, a convergence to a constant value of  $\approx \ln(2)$  is expected.

Note that  $k$  may be the same for different parameter combinations of  $E, D, \gamma, \dots$ . For example, the effect of a larger Young modulus can be balanced by the effect of a larger friction hence resulting in the same  $k$ . There is an alternative to the upper procedure to determine  $k$ . This is to perform many calculations to determine  $v(E, D, \dots)$  in the off-lattice model and use the relation  $v \approx \Delta R / \tau_e$  in order to determine  $k = \Delta R - 1$  from  $v$  (and  $\tau_e$ ).

The information on the initial exponential growth and the large-scale linear expansion can be used to collapse the growth curves for different  $k$  onto a single curve. By rescaling the  $y$ -axis in Fig. 6(b) according to  $R \rightarrow R / \Delta R$  and shifting the time axis by the crossover time as  $t \rightarrow (t - t_{cr}) / \tau$ , where  $t_{cr}$  results from  $2\Delta R = L_{cr} = 0.5l \exp(t_{cr} / (\tau_e 2))$ , the growth curves for different  $k$  collapse on a single curve. The range of velocities then is  $v > 0.25 \mu\text{m/h}$  (for e.g.  $l = 8 \mu\text{m}$ ,  $\tau = 12 \text{h}$ ). The data collapse in Fig. 7(b) can be used to simulate larger systems sizes or speed up the simulations for a given system size. This may be important if either experiments should be analyzed by computer simulations or if the effect of therapy on expanding monolayers should be studied [27]. If, for example, the experimental growth velocity suggests  $\Delta R = v\tau_e = k + 1$  with  $k \gg 0$ , one may, instead of simulating a growing monolayer using  $k$ , simulate a growing monolayer using  $k' = 1 \ll k$  ( $\Delta R' = 2$ ) and later upscale the growth curve obtained for  $k' = 1$  according to  $R \rightarrow (\Delta R)R / (\Delta R')$ ,  $t \rightarrow t + t_{cr}$  in order to obtain the growth curve for  $k$ , i.e. a patch of cells of edge length  $k + 1$  is represented by a small patch of “effective cells” of edge length  $k' + 1$ . Hence, while the original patch contained  $(k + 1) \times (k + 1)$  cells, the coarse grained patch contains  $(k' + 1) \times (k' + 1)$  effective cells, where each effective cell represents  $(k + 1)^2 / (k' + 1)^2$  true cells. Since the simulation time is  $\mathcal{O}(N)$  and  $N \propto R^2$ , this leads to a speed up of the simulation by a factor of  $(k + 1)^2 / (k' + 1)^2$  (e.g. 25 for  $k = 9$ ,  $k' = 1$ ). However, since for small  $k'$  lattice anisotropies appear in the monolayer geometry (Fig. 4(a)),  $k$  should not be chosen too small (usually  $k' > 0$  is sufficient).

### 3.1.2. Delauney Triangulation

The problem of lattice anisotropies may be circumvented by using a random lattice instead of a regular square lattice (Fig. 8). Here, in a first step, a regular square lattice is generated. Then, points are randomly placed into the squares of the lattice such that each lattice compartment contains precisely one point. These points are used to construct a Delauney Triangulation. Note that this choice of the construction points is important to insure translation invariance of the average cell size and homogeneity, and to avoid cell shapes deviating significantly from a compact shape that otherwise is likely to be observed if the construction points were randomly placed into the space. The Delauney Triangulation is the dual graph to the Voronoi Diagram, which has been used by Kansal *et al.* [47] to model brain tumor growth; unfortunately, their approach violates translation invariance. The monolayer growth process is then modeled on the Delauney Triangulation using

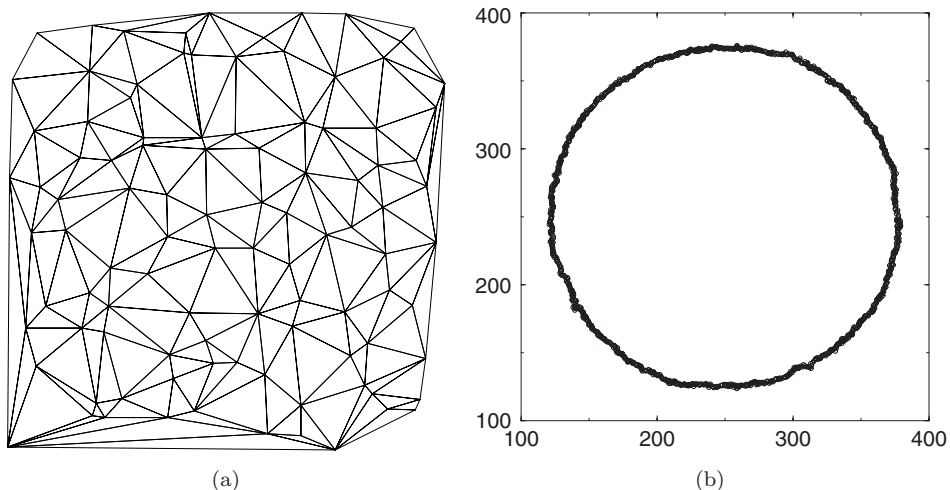


Fig. 8. In a random lattice, lattice asymmetries due to noise-reduction at large  $m$  do not emerge. (a) shows a Dirichlet Triangulation where initially one point has been placed at random into each square of a (regular) square lattice, i.e.  $M^2$  points for a  $M \times M$ -lattice. The Dirichlet Triangulation is the dual graph of the “Voronoi Diagram.” The nodes of the Dirichlet Triangulation represent the construction points of the Voronoi Diagram. In a Voronoi Diagram that region in space is assigned to a (construction) point that is closer to this point than to any other point. The Dirichlet Triangulation links each of the construction points of the Voronoi Diagram to its neighbor construction points. Our initial choice of point positions insures that the final shape of each Voronoi region does not deviate too much from a compact shape. (b) shows a simulation with  $m = 60$  up to  $N = 100,000$  cells. Note that no lattice artifacts occur in the monolayer geometry while in the case of a square lattice and  $m = 60$ , we did observe significant lattice effects (compare to Fig. 4(a)).

the rules of the CA-model above. In this case, the lattice anisotropies disappear even for large  $m$  and  $k = 0$  (compare Fig. 4 with Fig. 8). From the construction rules of the Delauney Triangulation, the average number of neighbors of a cell in two spatial dimensions is six, and the diagram is space filling. Alternatively, one could operate on a lattice in which the cell size is confined by an upper bound (e.g. by drawing a circle of radius  $\tilde{R}$  around the Dirichlet construction point and considering the space outside this circle as not being part of the cell; compare Refs. 25 and 28).

### 3.2. CA in the presence of free diffusion

In the presence of free diffusion, the surface of the monolayer is no longer sharp. In this case, a robust measure for the spatial spread is the radius of gyration:

$$R_{\text{gyr}} = \sqrt{\frac{1}{N} \sum_{i=1}^N (r_i - R_{\text{cm}})^2}, \quad (11)$$

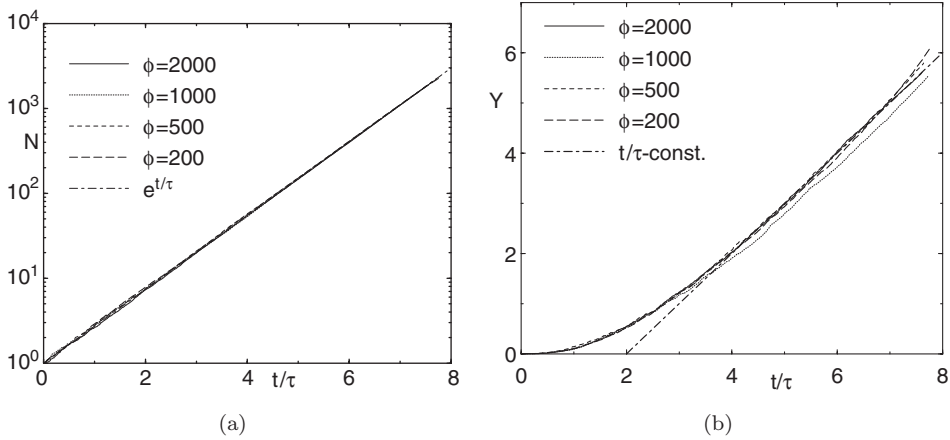


Fig. 9. Initial growth kinetics in the case of free diffusion with  $\phi = 200, 500, 1,000, 2,000$ . (a) Initially  $N \propto \exp(t/\tau)$ . (b)  $Y = R_{\text{gyr}}^2/(\lambda + \phi)$  versus  $t/\tau$ .

where  $\underline{R}_{\text{cm}} = \sum_{i=1}^N \underline{r}_i$  is the position of the center of mass. For a compact circular cell aggregate,  $R_{\text{gyr}}$  is related to the radius  $R$  of the aggregate by

$$R_{\text{gyr}} = R/\sqrt{2}. \tag{12}$$

In the presence of free diffusion, the initial population growth is again exponentially fast (Fig. 9(a)) while, however, the expansion is  $R_{\text{gyr}} \approx \sqrt{(\lambda + \phi)t}$  with  $\lambda = 1/\tau_e$  (Fig. 9), i.e. in the limit of negligible cell–cell interaction, cell division behaves as cell hopping. This view is supported by the observation that in the case of cell–cell interaction being completely suppressed (by allowing that each lattice site is occupied by more than one cell) the spread is  $R_{\text{gyr}} = \sqrt{\lambda t}$ . Note that the initial shoulder observed in Fig. 9 disappears for  $N(t = 0) \gg 1$  (Fig. 11). On large time scales, the expansion of the monolayer is again linear (Fig. 10). This can be explained as follows. In the exponential growth regime, free space is depleted exponentially fast while the spread of the monolayer is only  $\propto \sqrt{t}$ . Hence, the cells do not move sufficiently fast to permit exponential growth forever.

However, on large time scales the expansion of the monolayer is again linear in time,  $R \propto t$ . A CA with free hopping ( $\phi > 0$ ) corresponds to an off-lattice model without cell–cell adhesion ( $V_{ij}^{\text{attr}} = 0$ ). The simulations with free diffusion are very time-consuming, and the systematic parameter sensitivity for the off-lattice model in this case is not feasible. Here, the CA helps to analyze the qualitative dynamics in the parameter space spanned by  $(k, \lambda, \phi)$  as illustrated in Fig. 12. Note that  $v^2 \propto \phi$  and  $v \propto \Delta R$ . As shown in Fig. 12, for general  $\phi \geq 0$  and  $\Delta R > 1$ , the numerical simulations suggest for the asymptotic growth velocity the relation

$$v^2 \approx 0.94\Delta R^2 + 1.5\phi. \tag{13}$$

For  $\Delta R = 1$ , however, we found  $v^2 \approx 1.58 + 1.5\phi$ , that is, a larger velocity than suggested by Eq. (13), which may arise from the rougher surface structure observed

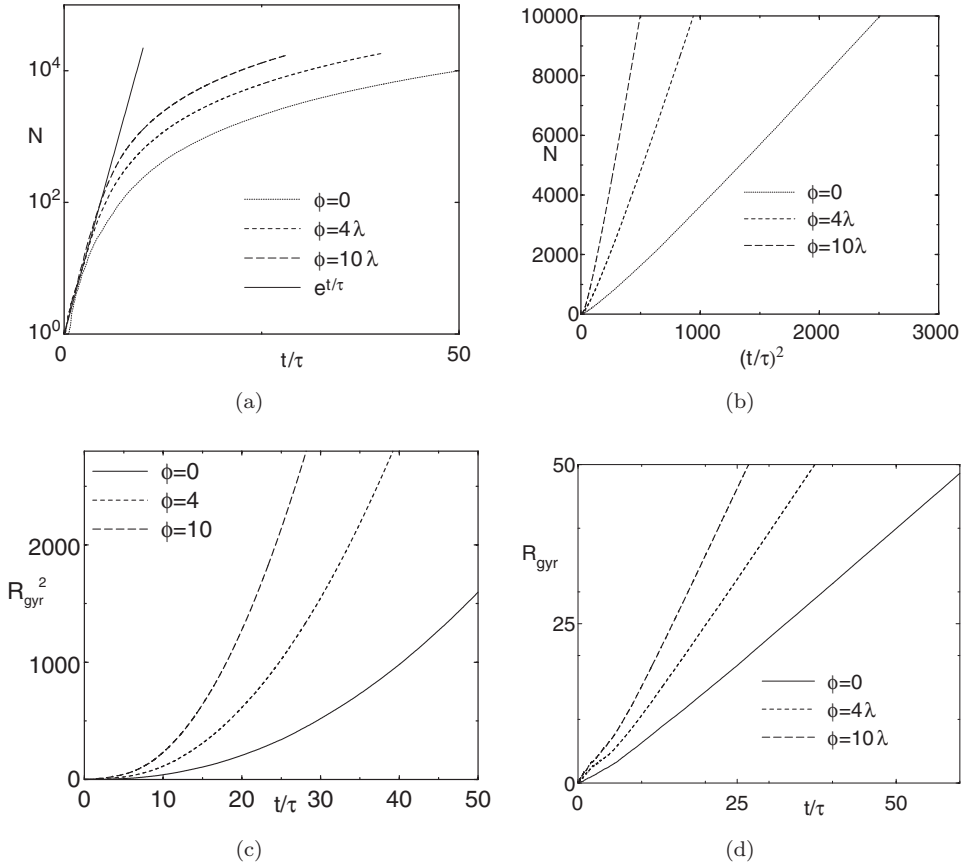


Fig. 10. Growth and spatial spread of cell populations in monolayers. Variation of  $\phi$ . (a) Initially the population size  $N$  grows exponentially fast. (b) The plot of  $N$  versus  $(t/\tau)^2$  shows that for large times,  $N \propto t^2$ . (c)  $R_{\text{gyr}}^2$  is no longer  $\propto t$ . As shown in (d)  $R_{\text{gyr}} \propto t$ , indicating a traveling wave behavior of the tumor border for large times as for a compact monolayer.

for  $\Delta R = 1$  resulting in more growth sites. (Note that all quantities are expressed in multiples of  $\tau$  and  $l$ .) In the case where  $\phi = 0$ , this is

$$v = \frac{dR}{dt} = \sqrt{2} \frac{dR_{\text{gyr}}}{dt} \approx \frac{\Delta R}{\tau}. \quad (14)$$

(In the last equation, we have put  $\tau$  although it is equal to one in scaled units.) For  $\phi \gg \lambda \Delta R^2$ ,

$$v^2 \propto \phi. \quad (15)$$

#### 4. Continuum Model

As reported in the introduction, for some biological situations rigorous coarse graining techniques starting from the microscopic scale of individual cells (or particles)

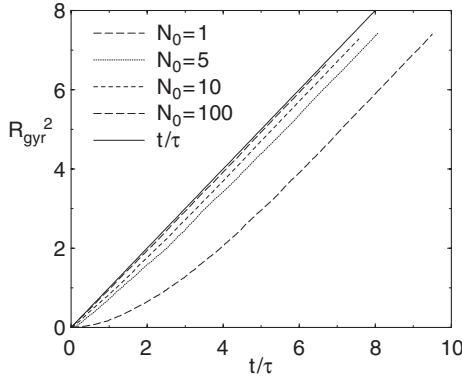


Fig. 11. Initial growth kinetics in the case of no exclusive-volume interaction for  $N(0) = 1, 5, 10, 100$  cells initially situated at the same lattice site, i.e. for the simulations in this figure, many cells are allowed to occupy the same lattice site and cells do not interact. Further,  $\phi = 0$ . The simulation shows that the shoulder that is observed for small  $N(0)$  disappears for large  $N(0)$ .

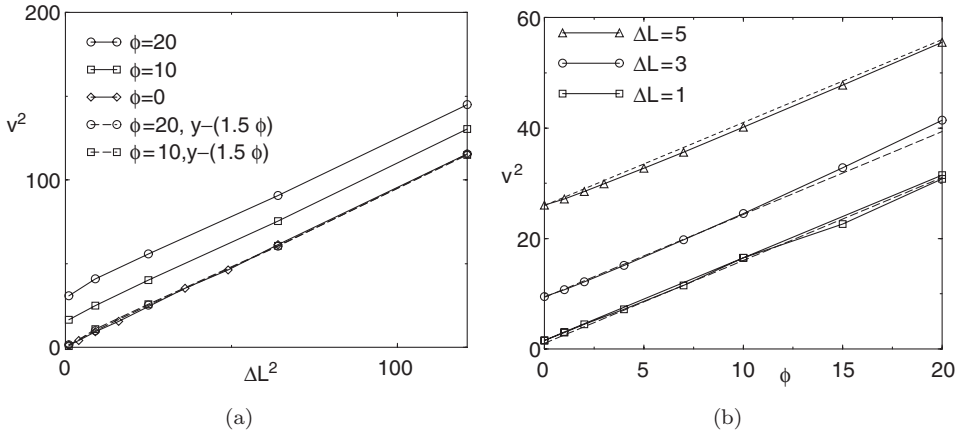


Fig. 12. (a) Square of asymptotic growth velocity  $v^2$ ,  $v = dR/dt$  of monolayer radius  $R$  versus  $\Delta R^2$  ( $\Delta R = k + 1$ ) for various  $\phi$ . (b)  $v^2$  versus  $\phi$  for various  $k$ . The findings suggest  $v \propto \Delta R$  and  $v \propto \sqrt{\phi}$ .

and ending up with descriptions for the average cell (or particle) density have been successfully applied. In Ref. 70, cells move stochastically with chemotactic drift on average into directions of an increasing cAMP molecule concentration. cAMP molecules move randomly, are released by cells and decay due to a death process. Both, cells and molecules are modeled by Langevin equations. In the limit of large cell (and molecule) numbers  $N$ , the stochastic contribution becomes irrelevant: as shown by mathematically rigorous error estimation, even at moderate  $N$  deterministic equations for local densities of the cells and the molecules give an excellent description of the process. The limiting equations are of the Keller–Segel type. The limiting procedure here is successful since the interaction is not completely local

but “moderate” i.e. the cell–cell interactions decay sufficiently fast in space and the interaction range (given e.g. by the width of an interaction weight function) scales in an appropriate way with the particle number [70]. Another example for competing cell populations introduced by Luckhaus and Triolo [54] and De Masi *et al.* [21] has already been briefly discussed in the introduction. In their approach, a rigorous limit is possible since the fast diffusion locally smoothes the cell density.

Here, we are faced with the problem of no (or almost no) diffusion and contact-inhibited cell division. We approach this problem by a formal ansatz which is motivated by a coarse graining procedure used for chemical equations [15, 63]. Formally this approach assumes local homogeneity and isotropy as well. However, here we also explore how far this approach captures the qualitative behavior of the expanding monolayer in the case of  $\phi = 0$ . In this approach, the rules of the cellular automaton are expressed as a set of “chemical reactions” which then are the starting point for a procedure from which approximate stochastic continuum equations can be derived [15, 33]. The approach does not consider the position of each individual cell anymore but focuses on spatial compartments which are large compared to an individual cell but small compared to the final population size of  $\sim 10^5$ – $10^6$  cells, and hence may contain many cells. Consequently multicellular configurations on spatial scales smaller than the compartment size cannot be distinguished anymore which, as shown below, is reflected by the resulting continuum equations. We firstly consider one space dimension and then generalize to  $d$  dimensions. On a spatial scale which is large compared to the size of single cells but small compared to the system size, the stochastic spatio-temporal dynamics of the growing multicellular system can be modeled by a compartment master equation for the multivariate probability  $p(x_1, x_2, \dots; t)$  of finding  $x_1$  cells in the spatial compartment 1,  $x_2$  cells in the spatial compartment 2, etc. at time  $t$ . The master equation is a first order linear equation for the probability density and can be written as a linear operator equation. The linear operator can be expressed in the language of second quantization, and the linear operator equation can be formally solved. The solution can be expressed as a path integral that describes the time development of the probability of particle configurations. In the continuum limit, an observable with respect to the probability density  $p$  (expressed in terms of an operator  $\Phi$ , see below) is given to leading order by the solution of a stochastic partial differential equation for the local cell density.

The system of “chemical reaction equations” has to represent cell migration and division. Motivated by the observation in the lattice model (see previous section) that the division of a cell to a neighbor site may be subdivided into two separate steps, a division within the same compartment (in the following denoted as “site”) followed by an immediate hopping step of the cell onto a neighbor site, we split the cell division into two reactions where one is written as an effective hopping step. The reactions reads:



$$X_i \xrightarrow{\bar{d}_{ij}} X_j \quad (A = 3), \tag{18}$$

$$X_i \xrightarrow{\zeta} 0 \quad (A = 4). \tag{19}$$

$A$  denotes the reaction number,  $X_i$  the number of cells at lattice site  $i$ .  $A = 1$  denotes cell division on the same lattice site.  $A = 2$  denotes the situation that one of the daughter cells immediately moves from site  $i$  to site  $j$  such that  $A = 1$ ,  $A = 2$  together model cell division on a site, and to a neighbor site.  $A = 3$  denotes a hopping process to a neighboring compartment. We included hopping here ( $A = 3$ ) since the technique formally requires homogeneity and isotropy within each spatial compartment and hopping smooth out the tumor-environment interface.  $A = 4$  denotes a cell death process (e.g. as a consequence of drug treatment). The spatial dependency has been taken into account by dividing the space into square compartments of equal size with a lattice spacing  $b \gg l$ , where  $l$  is the cell size. Accordingly,  $\tilde{N} = b^d/l^d$  is the total number of cells that would fit into a spatial compartment (site) ( $\forall i$ ). For simplicity, we set in the following  $l = 1$ . In order to account for the fact that no cell division or hopping can occur anymore if the compartment into which the division or hopping should take place is full (i.e. has  $\tilde{N}$  cells), we set  $\bar{\lambda} = (1 - X_i/\tilde{N})\lambda$ ,  $\bar{\omega}_{ij} = (1 - X_j/\tilde{N})\omega_{ij}$  and  $\bar{d}_{ij} = (1 - X_j/\tilde{N})d_{ij}$ . Hence, at a first glance the above system of “reactions” seems to give a reasonable description of the growth process. In addition since the reaction  $A = 2$  models the physical situation that a cell division can only take place if sufficient free space is available, reactions  $A = 1, 2$  are inherently linked. Hence, the reaction rate  $\omega_{ij}$  is a function of  $\lambda$ . We assume  $d_{ij} \neq 0$  and  $\omega_{ij} \neq 0$  only, if  $i, j$  are neighbor compartments (NNs). Further, we assume that  $d_{ij} = \phi/(2d\tilde{b}^2)$  for  $i, j$  NNs, where  $\phi$  is the jump rate and  $\tilde{b} = b/l$ . This choice insures that a choice of a larger compartment size is related with a reduction of the jump rate such that the true diffusion length does not depend on the choice of the compartment size. The relation between  $\omega_{ij}$  and  $\lambda$  can be constructed either *a posteriori* or *a priori*. We construct it here *a priori* and assess it *a posteriori*. We assume that a particle generated with rate  $\lambda$  jumps with a rate  $\omega_{ij} = \lambda/(2d\tilde{b}^d) \neq 0$  if  $i, j$  are neighboring lattice sites. The similarity to the relation for  $d_{ij}$  reflects that cell division of a cell at lattice site  $i$  to a neighbor site can be interpreted as a division from a cell at site  $i$  onto the (same) site  $i$  followed by a hop to a neighbor site  $j \neq i$  as explained above (see Fig. 11).

The full master equation (for simplicity in  $d = 1$ ) reads (using the method in Ref. 36):

$$\begin{aligned} \frac{\partial p(\underline{x}; t)}{\partial t} = & \sum_i \frac{\lambda}{\tilde{N}} [(x_i - 1)(\tilde{N} - (x_i - 1))p(x_i - 1, \hat{\underline{x}}; t) - x_i(\tilde{N} - x_i)p(\underline{x}; t)] \\ & + \sum_i \sum_j \frac{\omega_{ij}}{\tilde{N}} [(x_i + 1)(\tilde{N} - (x_j - 1))p(x_i + 1, x_j - 1, \hat{\underline{x}}; t) \\ & - x_i(\tilde{N} - x_j)p(\underline{x}; t)] \end{aligned}$$

$$\begin{aligned}
 & + \sum_i \sum_j \frac{d_{ij}}{\tilde{N}} [(x_i + 1)(\tilde{N} - (x_j - 1))p(x_i + 1, x_j - 1, \hat{\underline{x}}; t) \\
 & - x_i(\tilde{N} - x_j)p(\underline{x}; t)] \\
 & + \sum_i \zeta [(x_i + 1)p(x_i + 1, \hat{\underline{x}}; t) - x_i p(\underline{x}; t)]. \tag{20}
 \end{aligned}$$

The master equation is linear in the probability and can formally be written as a linear operator equation:

$$\frac{d|\hat{\Phi}(t)\rangle}{dt} = -H|\hat{\Phi}(t)\rangle \tag{21}$$

with the state vector

$$|\hat{\Phi}(t)\rangle = \sum_{\{x_i\}} p(\underline{x}_i; t) |x_i\rangle \tag{22}$$

$$= \sum_{\{x_i\}} p(\underline{x}_i; t) (a_1^+)^{x_1} (a_2^+)^{x_2} \dots (a_i^+)^{x_i} \dots |0\rangle. \tag{23}$$

$\{x_i\} = \{x_1, \dots, x_i, \dots, x_N\}$ ,  $\underline{x}_i = (x_1, \dots, x_i, \dots, x_N)$ . The  $a_k^+$  are creation operators,  $|0\rangle$  is the vacuum state (no cell) of the multi-particle system with

$$a_i^+ |x_1, \dots, x_i, \dots, x_N\rangle = |x_1, \dots, x_i + 1, \dots, x_N\rangle. \tag{24}$$

We further define the annihilation operator  $a_k$  by

$$a_i |x_1, \dots, x_i, \dots, x_N\rangle = x_i |x_1, \dots, x_i - 1, \dots, x_N\rangle, \tag{25}$$

and require that the (bosonic)-like operators obey the commutation relations

$$[a_i, a_j^+] = a_i a_j^+ - a_j^+ a_i = \delta_{ij}. \tag{26}$$

This *ansatz* can be used to derive a continuum equation for the cell density. The line of reasoning is as follows. (Details on the calculation steps can be found in Appendix B.) The ‘‘Hamiltonian’’  $H$  can be expressed in combinations of the creation and annihilation operators where the annihilation operators have to be on the right-hand side of the creation operators (‘‘normal order’’). The operator equation then can formally be solved for any observable. The solution can be expressed as a path integral that describes the time development of the probability of particle configurations. For this purpose, the path integral is formulated in terms of coherent states and their complex conjugates. Coherent states are eigenstates of the annihilation operator. The eigenvalues of the annihilation operators are later related to the density of the cells  $n$ , the eigenvalues of the creation operators later to an auxiliary-field  $\tilde{n}$ . On large spatial scales, the coupling constants (pre-factors) of the higher-order non-linearities  $\sim n^p \tilde{n}^q$  ( $q + p > 3$ ) that appear in the continuous action may be neglected [45]. Collecting only terms up to second order in the auxiliary field, one obtains after integration over the auxiliary field a stochastic differential

equation for the local cell density (in  $d$  dimensions):

$$\frac{\partial n(\underline{x}, t)}{\partial t} = (b^2 D + b^2 \omega) \Delta n(\underline{x}, t) + (\lambda(1 - n(\underline{x}, t)) - \zeta) n(\underline{x}, t) + \sqrt{2\lambda n(\underline{x}, t)} \eta(\underline{x}, t). \tag{27}$$

$\eta(\underline{x}, t)$  models white noise with  $\langle \eta(\underline{x}, t) \rangle = 0$  and  $\langle \eta(\underline{x}, t) \eta(\underline{x}', t') \rangle = \delta(t - t') \delta(\underline{x} - \underline{x}')$ . Here,  $b$  is the lattice spacing. Now, we re-insert our original parameter choice:

$$\omega = \frac{\lambda}{2\tilde{d}b^2}, \tag{28}$$

$$D = \frac{\phi}{2\tilde{d}b^2}, \tag{29}$$

and obtain

$$\frac{\partial n(\underline{x}, t)}{\partial t} = l^2 \frac{\lambda + \phi}{2d} \Delta n(\underline{x}, t) + (\lambda(1 - n) - \zeta) n(\underline{x}, t) + \sqrt{2\lambda n(\underline{x}, t)} \eta. \tag{30}$$

*Small cell density:* If the cell density is small ( $n \ll 1$ ) the non-linearities can be neglected and the equation becomes

$$\frac{\partial n(\underline{x}, t)}{\partial t} = l^2 \frac{\lambda + \phi}{2d} \Delta n(\underline{x}, t) + (\lambda - \zeta) n(\underline{x}, t) + \sqrt{2\lambda n(\underline{x}, t)} \eta. \tag{31}$$

$\tilde{b}$  is the lattice spacing referred to the cell diameter. Note that the corresponding mean-field equation can be solved exactly by Fourier transformation, which yields in the case of  $d = 2$  considered here  $n(\underline{x}, t) = n(\underline{0}, 0) \frac{1}{\sqrt{4\pi\tilde{D}t}} e^{(\lambda - \zeta)t} e^{-\frac{R'^2}{4\tilde{D}t}} = n(R', t)$

with  $\tilde{D} = l^2(\lambda + \phi)/4$ ,  $R'^2 = x^2 + y^2$ . The initial population size is given by integration over the position variables,  $N(t) = \int_{\Omega} n(\underline{x}, t) d^2 \underline{x}$  from which  $N(t) = N(t = 0) e^{(\lambda - \zeta)t}$  is obtained, i.e. precisely the initial growth behavior found for the CA in the presence of free diffusion (where  $\zeta = 0$ ). Note, however, that for  $\lambda \approx \zeta$ , the effect of the noise cannot be neglected and in particular for small population sizes can lead to extinction [56]. The spatial spread is

$$\begin{aligned} R_{\text{gyr}} &= \left( \frac{\int_{\Omega} (R')^2 n(\underline{R}', t) R' dR' d\varphi}{\int_{\Omega} n(\underline{R}', t) R' dR' d\varphi} \right)^{1/2} \\ &= \sqrt{2d\tilde{D}t} = \sqrt{l^2(\lambda + \phi)t} \end{aligned}$$

as found in the CA-simulations.

Note also that the parameter  $k (= \Delta R - 1)$  does not play a role in the interaction-free case. As shown below, the effect of non-Poissonian cycle times on the initial growth kinetics can be calculated analytically based on the same simple kinetic approach that we use here.

*Large cell density:* In the zero-noise limit (neglecting the last term in Eq. (30)) one obtains the classical Fisher-KPP-equation that has been extensively used in tumor modeling (see e.g. Ref. 74). In this limit, for the minimum wave velocity one obtains  $v_{\text{min}}^2 \geq 4l^2 \lambda \frac{\lambda + \phi}{2d}$ , i.e. for e.g.  $\phi = 0$  and  $d = 2$ ,  $v_{\text{min}} \geq l\lambda = l/\tau$  as in the CA-simulations (Fig. 7(a) for  $m = 1$ ). Hence, the Fisher-KPP-equation models

the process with Poissonian cycle times which becomes immediately apparent if one recalls that the above system of “chemical equations” (17)–(19) represents a Poisson process for each individual reaction. However, with the choice  $\lambda = 1/\tau \rightarrow \lambda = 1/\tau_e$ , where  $\tau_e = \tau/\ln(2)$ , a reasonable approximation also for the system with  $\delta$ -correlated noise may be obtained.

The case where a cell can push  $k$  cells aside may be compared to an “effective” cell that pushes one cell aside on a lattice with spacing  $(k+1)b = \Delta Rb$  (compare the description to Fig. 7(b) in the last section). Since this rescaling would effectively increase diffusion as well, the diffusion constant has to be rescaled according to  $D \rightarrow D/\Delta R^2$  in order to insure that the “true” diffusion is not affected. Doing so, the minimum wave speed increases by a factor of  $k+1$  (for  $\phi = 0$ ), which is the behavior observed in computer simulations with a single-cell based model, i.e.  $v_{\min}^2 \geq 4l^2\lambda \frac{\lambda\Delta R^2 + \phi}{2d}$ . Note, that for  $\phi = 0$  (no diffusion) one obtains  $v_{\min} \geq \lambda\Delta R = \Delta R/\tau$  as in our CA-simulations. That is, the large scale linear increase of the monolayer radius in the deterministic PDE shows the same behavior as in the CA simulations. At the same time, the stochasticity is covered to lowest order.

However, the minimal growth velocity for  $\phi \neq 0$ ,  $\Delta R > 1$  differs quantitatively from the value found in the cellular automaton simulations although the qualitative dependence ( $v^2 \propto \phi$ ,  $v \propto \Delta R$ ) is the same. This may have different reasons. Firstly, it should be noted that the asymptotic wave speed in cellular automaton simulations depends on the precise choice of the microscopic rules for hopping and cell division. This is not reflected by our “chemical reaction” equations for the cell dynamics. For illustration, consider a cell has been chosen for a hopping move. Let rule A be that the cell is moved with probability one in the case where it has at least one free neighboring lattice site. Let rule B be that one of the neighbor sites is chosen at random and the migration move is performed only if this lattice site is free. Hence, for rule A the asymptotic growth velocity is larger than for rule B (Fig. 13). Rule B is closer to the off-lattice model where we performed migration steps into a random direction independent on the local cell environment. However, also for this rule we did not find the precise wave velocity of the Fisher-KPP-equation (the observed expansion velocity is slightly below  $\sqrt{\lambda + \phi}$ ). Secondly, the noise term modifies the shape of the traveling wave front in particular at the front tip and is known to affect the expansion velocity (e.g. Refs. 11 and 23). In a next step, which is beyond the scope of this article, the numerical solutions of Eq. (30) should be directly compared to the simulation results of the lattice model using different rules.

An alternative description of the dynamics on the lattice could be based on a master equation for the division and hopping process in the lattice model following

$$\frac{\partial p(\{Z\}, t)}{\partial t} = \sum_{\{Z'\} \rightarrow \{Z\}} W_{\{Z'\} \rightarrow \{Z\}} p(\{Z'\}, t) - W_{\{Z\} \rightarrow \{Z'\}} p(\{Z\}, t), \quad (32)$$

where  $W(\{Z'\} \rightarrow \{Z\})$  denotes the transition rate from configuration  $\{Z'\}$  to configuration  $\{Z\}$ . Different from the master equation in this section,  $\{Z\}$  denotes a configuration of the original cellular automaton (of Sec. 3) and obeys the exclusion

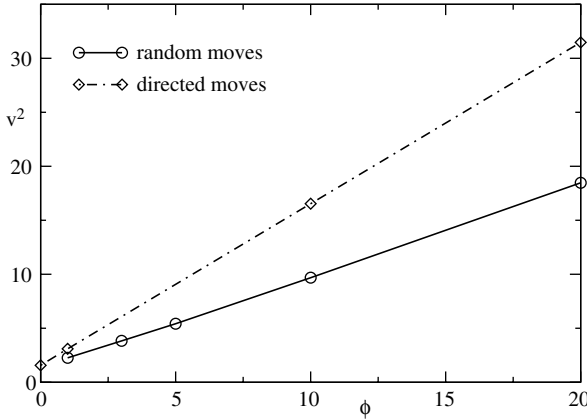


Fig. 13. Cell spreading velocity  $v = dR/dt$  for directed moves (rule A, see text) and random moves (rule B, see text). If a cell moves with probability one once if it has at least one free neighbor site (directed moves) then the spreading velocity of the expanding cluster is larger than if a cell tries to move with equal probability on one of its neighbor sites in which case a move is successful only if the chosen neighbor site is not occupied by another cell (random moves).

principle (i.e. maximal one cell at each lattice site). The configuration changes include hopping with rate  $\phi$ , division with rate  $\lambda$ , and, in the case of an Erlang-distributed cycle time intermediate transitions between the  $m$  states of an internal counter (see also next subsection). As an alternative to the algorithm we use in Sec. 3, the event time can, in this case, be determined by the Gillespie algorithm by

$$\Delta t = -\frac{1}{W_Z} \ln(1 - \xi),$$

where  $\xi \in [0, 1)$  is a random number. Here  $W_Z = \sum_{Z'} W_{\{Z\} \rightarrow \{Z'\}}$  denotes the transition rate from the global state  $\{Z\}$  into any state  $\{Z'\}$  of the system, and  $W_{\{Z\}}$  the rate with which the state  $\{Z\}$  can be left [67]. Note, that this implies that a particle that has more free neighbor sites on which it could hop to has a larger probability to move (than if it would have less free neighbor sites to hop onto). According to our above line of argument (see Fig. 13), this cannot be *a priori* expected for cells. Here, the rule may have to be modified such that the number of cells that can move, and not the number of potential target states, determines the event time (Block, Drasdo & Schöll, in preparation).

We have also studied other systems of “chemical reactions” and always obtained on large scales with the procedure explained in Appendix B the same form of continuum equation. Hence, the approximate equation is robust against details in the description of the cell hopping and division.

The stochastic effects become important, for instance, also in the case where death processes occur with a rate  $\zeta \approx \lambda$  for which the dynamics below the critical dimension of 4 is completely determined by the noise [14]. The deterministic

Fisher equation has often been used as a phenomenological continuum approach to growing multicellular systems. Its solution for long times correctly agrees with the numerical simulation results of both the cellular automaton and the off-lattice model. However, in the absence of a sufficiently fast cell diffusion for small times, the Fisher equation fails to give a correct description of the system behavior of the individual based systems for small times. Here, it predicts the radius grows as  $\langle R'(t) \rangle \propto \int R' n(R', t) (R')^{d-1} dR' / \int n(R', t) (R')^{d-1} dR' \propto \sqrt{t}$ , controlled by the quasi-diffusion term due to the division into neighbor compartments. On the other hand, the exponential growth of the population size  $N$  is correctly obtained. The deviation at small times is a consequence of the violation of homogeneity and isotropy within the individual compartments that occurs for  $\phi = 0$ . In the case of  $\phi \gg \lambda$ , the cell distribution is homogeneous and isotropic and the corresponding CA-simulations also show  $R \propto \sqrt{t}$ . One may consider  $R \propto N^{1/d}$  as a measure for the initial monolayer radius which on the one hand would insure exponential growth of  $R$  but on the other hand would fail in the case that “true” diffusion takes place. A method which is capable of reflecting the short time behavior could be based on a continuum mechanical approach, e.g. by approaching the tumor as a viscoelastic medium. As already argued above, the cell movement in expanding cell populations may have two origins: (i) passive pushing as a consequence of the proliferation pressure exerted by the proliferating cells, and (ii) active migration that occurs if the cell movement is a consequence of a stimulating signal by a growing neighbor cell. In case (i), it is the pressure gradient that guides the shift of cell mass. In case (ii), it is more active movement of cells initiated by the signal of a neighbor cell that may be triggered such that the cell attempts to maintain a certain migration speed similar to the movement of autonomous agents (e.g. vehicles) in traffic flow (see, for example, Helbing [40] and references therein, [41] and references therein). Consequently, similar limiting procedures starting from a Boltzmann-like approach may apply in this case. Note, however, that the Boltzmann equation (or Boltzmann-like equation as those used in traffic flow [40]) is based on a single particle distribution function for the velocity and the position of a single agent while the approach we have used here is based on the multivariate probability distribution that tracks the whole particle (here: cell) configuration and hence includes all correlations and fluctuations. Since it is usually difficult to consider higher-order correlations than pair correlations in Boltzmann-like equations, a systematic derivation of macroscopic (fluid-like) equations for the cell density from Boltzmann-like equations that include fluctuations and correlations remains a challenge. However, steps in the direction of linking the macro to the micro picture in this case have been performed, for example, by Stevens [70] and by Alt *et al.* [1].

In conclusion, Eq. (31) is a useful approximation to monolayer growth (i) in the presence of true diffusion ( $\phi > 0$ ) which insures local mixing, and (ii) in the linear expansion regime. The equation fails to give a proper qualitative description of the initial exponential growth regime of compact monolayers.

#### 4.1. Erlang cycle time distribution

As indicated by computer simulations, an Erlang-distributed cell-cycle time distribution results in a slower growth of the population size in the exponential growth regime. Following the same line of reasoning as above and taking into account that an Erlang-distributed cycle time can be obtained from a sum of Poissonian-distributed cycle times, i.e.  $\tau = \sum_{i=1}^m \tau_m$  with  $\langle \tau_m \rangle = \langle \tau \rangle / m$  (where  $\langle \dots \rangle$  denotes an average over many realizations of choosing the cycle time), the “chemical reaction equations” in the exponential regime read:

$$\begin{aligned}
 X^{(1)} &\xrightarrow{\lambda_1} X^{(2)}, \\
 X^{(2)} &\xrightarrow{\lambda_2} X^{(3)}, \\
 &\vdots \\
 X^{(m-1)} &\xrightarrow{\lambda_{m-1}} X^{(m)}, \\
 X^{(m)} &\xrightarrow{\lambda_m} 2X^{(1)}.
 \end{aligned} \tag{33}$$

The spatial index was dropped since in the exponential regime the cells do not interact such that the spatial coordinate can be integrated out. The corresponding set of first order differential equations  $dX^{(i)}/dt = \dots$  for the total number of cells in a cycle time compartment  $i$  can be formally solved with an *ansatz* of the form  $\vec{X} = \sum_{i=1}^m \vec{A}_i e^{\lambda_i t}$  yielding a matrix equation for the eigenvalues  $\lambda_i$ . For  $\lambda_i = m\lambda = m/\tau \forall i$ , the largest eigenvalue, which dominates the growth behavior, is readily calculated to

$$\lambda_{\max} = (2^{1/m} - 1)m/\tau. \tag{34}$$

For  $m = 1$ ,  $\lambda_{\max} = 1/\tau$ , and hence the population grows as  $N \propto e^{t/\tau}$  in the exponential regime. For  $m \rightarrow \infty$ ,  $e^{(2^{1/m}-1)mt/\tau} \rightarrow 2^{t/\tau}$ . Both are in agreement with the findings in the cellular automaton model (see Fig. 6).

## 5. Discussion

We have sketched how growing monolayers can be modeled at different levels of detail and used the experimental findings of Bru *et al.* [10] to guide our model development. As in the experiments we find an initially exponentially fast growing population size crossing over to a linear expansion of the population’s spatial spread at large times, which is triggered by contact inhibition, in our simulations induced by mechanical stress. We started by an approach where each cell was modeled by an elastic, sticky colloid-like particle of limited compressibility and deformability capable of active migration, growth and division. A cell is parameterized by characteristic geometrical, cell-biological, biophysical and cell-kinetic properties. We observed that this model that subsumes intracellular properties such as the cytoskeleton, adhesion molecules, the cell cycle, etc. in effective parameters is capable of giving a quantitative description of growing monolayer cultures. However, the

limitation of this approach is that it is computationally too demanding to permit a systematic exploration of the parameter space up to large system sizes with a reasonable effort, and to model system sizes that correspond to typical *in vivo* systems such as tumors. This, however, can be achieved by the cellular automaton model. The challenge of the cellular automaton model is to choose the rules properly in order to represent the correct physics and biology. We have chosen the CA rules being guided by our findings in the off-lattice model, which represents a more direct approach to a multicellular system and hence is believed to be closer to reality. We proposed introducing an additional parameter that controls the size of the proliferating rim to account for the experimentally observed velocity variations. The larger the proliferating rim is and, for a given intrinsic cell cycle time, the broader the cycle time distribution is, the larger the velocity of spatial spread. Since at a small proliferating rim size for sharply peaked cycle times (as typically found in experiments) the monolayer geometry reflects lattice artifacts from the underlying rectangular lattice symmetry, we propose to use in this case a Dirichlet Tessellation which does not show any spatial artifacts. In a next step, we have analyzed the situation in which the mobility of the cell is large and cell–cell adhesion is negligible. In this case, the initial spread of the cell population is  $\propto \sqrt{t}$  while for long times the expansion is again linear in  $t$  as for compact monolayers. In a last step, we looked at an even larger scale where cells were not considered as individual particles anymore, but instead by a locally averaged cell density. To maintain the inherent stochasticity of the growth process, we used a procedure that has been considered for chemical reactions to obtain a large scale descriptions of stochastic many particle systems. Strictly applied, this technique assumes a homogeneous distribution of cells within spatial compartments which are large compared to cells, but interestingly, we found a remarkable similarity between the large-scale properties of the equation that resulted from this procedure from the stochastic process even in the absence of diffusion. However, to tie this link more closely in a next step, simulation results with the cellular automaton model should be compared quantitatively to the numerical solutions of the continuum equation. This should imply extending the continuum approach presented in order to capture the initial exponential expansion of the monolayer diameter for compact monolayers.

The procedure outlined in this paper may open the possibility to calibrate large-scale simulations in small systems and then upscale to system sizes of interest. The same line of reasoning as shown in this paper for monolayers can be followed in the case of tumor spheroids. In this case, the tumor cell population size is partly controlled by the supply of nutrients or growth factors which have to be considered in a separate reaction–diffusion equation. However, the expansion of the tumor diameter can again be explained by the same biomechanical form of contact inhibition as used in this paper to explain the expansion of compact monolayers [26]. Even *in vivo* growing tumor Xenografts may follow the same growth scenario that is presented here (unpublished results). The ultimate goal could be the computer-based optimization of cancer therapy. We believe individual-based models will also

be needed for large multicellular systems, since therapy effects may introduce large spatial-temporal fluctuations in a tumor such that locally a resolution on the cellular level may be required.

### Acknowledgment

The author thanks A. Stevens and H. Schwetlick for helpful discussions at an early phase of the project. He is particularly grateful to A. Stevens for explaining challenges and limitations of important multi-scale approaches; M. Block and N. Jagiella for the adaption of a program to generate Fig. 6; and useful discussions with Jörg Galle. The simulations in Sec. 2.1 were performed with software by Dirk Drasdo and Stefan Höhme. Finally, the author thanks A. Krinner for a critical reading of the paper. The work was partly supported by DFG Grant No. BIC-6 1/1.

### Appendix A. Orientation Changes

For non-spherical objects, the torque has to be considered in addition to the force on the center of mass. The angular momentum  $\underline{J}_i$  of cell  $i$  with respect to its center of mass is

$$\underline{J}_i = \int_{V_i} \varrho(\underline{r}_i^c) (\underline{r}_i^c \times \underline{v}_i^c), d^d \underline{r}, \quad (\text{A.1})$$

where  $\varrho$  is the material density.  $\underline{r}^c = \underline{r} - \underline{r}_{\text{cm}}$  with  $\underline{r}_{\text{cm}} = \int_{S_{\text{cell}}} \varrho(\underline{r}, t) \underline{r} d\underline{r} / \int_{S_{\text{cell}}} \varrho(\underline{r}, t) d\underline{r}$  being the position of the center of mass. The angular momentum  $\underline{\Omega}_i = \underline{r}_i^c \times \underline{v}_i^c$  of cell  $i$  obeys the equation of motion

$$\frac{d\underline{J}_i}{dt} = \frac{d(\underline{I}_i \underline{\Omega})}{dt} = -\underline{\gamma}_{\text{r}}^{cs} \underline{\Omega}_i - \underline{\gamma}_{\text{r}}^{cc} \sum_j \underline{r}_i^{ij} \times (\underline{v}_j^{ij} - \underline{v}_i^{ij}) + \underbrace{\int_{V_i} \underline{r}_i^{(c)} \times \underline{f}_i d^d \underline{r}}_{\hat{\underline{\tau}}_i} + \hat{\underline{\tau}}_i. \quad (\text{A.2})$$

Here,

$$[I]_i^{lj}(t) = \int_V \varrho(\underline{r}_i, t) ((r_i^c)^2 \delta_{lj} - (r_i^c)^l (r_i^c)^j) d^3 \underline{r}, \quad (\text{A.3})$$

is the inertia tensor for cell  $i$ .  $\hat{\underline{\tau}}_i^\xi$  is the fluctuating torque on cell  $i$  with  $\langle \hat{\underline{\tau}}_i^\xi(t) \rangle = \underline{0}$  and autocorrelation

$$\langle \hat{\underline{\tau}}_i^\xi(t) \hat{\underline{\tau}}_i^\xi(t') \rangle = \underline{\underline{G}}_r \delta(t - t'). \quad (\text{A.4})$$

$\underline{\underline{G}}_r$  here is a matrix and quantifies the amplitude of the autocorrelation function of the random orientation fluctuations. In the case of friction-dominated dynamics, the term  $\frac{d\underline{J}}{dt}$  can be neglected.  $\underline{f}_i$  is the force density on cell  $i$ . For simplicity, we make a number of simplifying assumptions.

We approximate the cells in the mitosis phase by a dumb-bell as in Fig. 1 and assume the mass is concentrated in the spheres of the dumb-bell. Then the torque on cell  $i$  becomes

$$\hat{\boldsymbol{\tau}}_i = \frac{a}{2} \hat{\boldsymbol{a}} \times (\underline{\boldsymbol{F}}_i^{(1)} - \underline{\boldsymbol{F}}_i^{(2)}). \quad (\text{A.5})$$

Here,  $a$  is the axis length of the dumb-bell,  $\underline{\boldsymbol{F}}_i^{(1)}$  the force on one,  $\underline{\boldsymbol{F}}_i^{(2)}$  on the other sphere of the dumb-bell. The angular velocity  $\underline{\boldsymbol{\Omega}}_i$  can be related to the time derivative of the direction vector  $\hat{\boldsymbol{a}}_i$  by

$$\frac{d\hat{\boldsymbol{a}}_i}{dt} = \underline{\boldsymbol{\Omega}}_i \times \hat{\boldsymbol{a}}_i \quad (\text{A.6})$$

$$\Leftrightarrow \underline{\boldsymbol{\Omega}}_i = \hat{\boldsymbol{a}}_i \times \frac{d\hat{\boldsymbol{a}}_i}{dt}. \quad (\text{A.7})$$

Since in the friction-dominated regime,  $d\underline{\boldsymbol{J}}_i/dt$  may be neglected, the equation for the angular momentum becomes an equation for the angular velocity  $\underline{\boldsymbol{\Omega}}_i$  and, by Eq. (A.7), an equation for the temporal development of the dumb-bell director.

The calculations for the rotational friction matrices  $\underline{\underline{\gamma}}_r^{cc}$  and  $\underline{\underline{\gamma}}_r^{cs}$  can be very complex (see, for example, Ref. 22 for rotating rods in a homogeneous medium). For a dumb-bell, the rotation along the long axis may not need to be considered. However, the rotation around the axis perpendicular to the long axis needs to be taken into account (the axis should intersect the dumb-bell axis at the center of mass). The friction coefficient with respect to this axis may be approximated as follows. For spheres in a fluid,  $\underline{\underline{\gamma}}_r^{cs} = \gamma_r^{cs} \hat{\boldsymbol{I}}$  with  $\gamma_r^{cs} = 8\pi\eta_0 \tilde{R}^3$  (a scalar), where  $\eta_0$  is the shear viscosity of the surrounding (fluid) medium. For long thin rods, for which the rod length  $L \gg \tilde{R}$ , where  $\tilde{R}$  is the rod radius,  $\gamma_r^{cs} = \pi\eta_0 L^3 / (3 \ln(L/(2\tilde{R})))$  is the friction coefficient for rotations around the axis perpendicular to the rod axis through the center of mass. For a dumb-bell, the rotational coefficient is not known. Comparing with the rod, we may approximately write for a dumbbell  $L = 2\tilde{R} + a$ , where  $a$  is the length of the dumb-bell axis. Since for cells  $0 \leq a \leq 2\tilde{R}$ , we need an approximative relation for  $\gamma_r^{cs}$  which we construct in such a way that in the limit  $a \gg \tilde{R}$ , we obtain the long rod-limit. Along this line of argument  $\gamma_r^{cs}$  may be estimated as  $\gamma_r^{cs} \approx \pi\eta_0 (2\tilde{R} + a)^3 / (2\tilde{R}/(2\tilde{R} + a) + 3 \ln((a + 2\tilde{R})/(2\tilde{R})))$ . This approximation correctly reproduces the perfect-sphere-limit if  $a = 0$  and the (formal) limit of long rods  $L \equiv a + 2\tilde{R} \gg \tilde{R}$ . The translation friction coefficients  $\gamma_{\parallel}^{cs}$  and  $\gamma_{\perp}^{cs}$  (see Eq. (5)) can then be approximated by  $\gamma_{\parallel}^{cs} \approx 2\pi\eta_0 (3\tilde{R} + a) / (2\tilde{R}/(2\tilde{R} + a) + \ln((a + 2\tilde{R})/2\tilde{R}))$ , which yields the sphere-limit  $\gamma_{\perp}^{cs} = \gamma_{\parallel}^{cs} = 6\pi\eta_0 \tilde{R}$  in the case of  $a = 0$  and the long-rod limit in the case of  $a \gg 2\tilde{R}$ .  $\gamma_{\perp}^{cs} \approx 2\pi\eta_0 (3\tilde{R} + 2a) / (2\tilde{R}/(2\tilde{R} + a) + \ln((a + 2\tilde{R})/2\tilde{R}))$ . For  $a \gg 2\tilde{R}$ ,  $\gamma_{\perp}^{cs} = 2\gamma_{\parallel}^{cs}$  [22].

### Appendix B. From a Population Master Equation to the Continuum

Here, we give the detailed derivation of the stochastic differential equation from the multivariate master equation (20) for the local cell number.

The master equation is linear in the probability and can formally be written as a linear operator equation:

$$\frac{d|\hat{\Phi}(t)\rangle}{dt} = -H|\hat{\Phi}(t)\rangle \tag{B.1}$$

with the state vector

$$|\hat{\Phi}(t)\rangle = \sum_{\{x_i\}} p(\underline{x}_i; t) |\underline{x}_i\rangle \tag{B.2}$$

$$= \sum_{\{x_i\}} p(\underline{x}_i; t) (a_1^+)^{x_1} (a_2^+)^{x_2} \dots (a_i^+)^{x_i} \dots |0\rangle. \tag{B.3}$$

$\{x_i\} = \{x_1, \dots, x_i, \dots, x_N\}$ ,  $\underline{x}_i = (x_1, \dots, x_i, \dots, x_N)$ . The  $a_k^+$  are creation operators,  $|0\rangle$  is the vacuum state (no cell) of the multi-particle system with

$$a_i^+ |x_1, \dots, x_i, \dots, x_N\rangle = |x_1, \dots, x_i + 1, \dots, x_N\rangle. \tag{B.4}$$

We further define the annihilation operator  $a_k$  by

$$a_i |x_1, \dots, x_i, \dots, x_N\rangle = x_i |x_1, \dots, x_i - 1, \dots, x_N\rangle, \tag{B.5}$$

and require that the (bosonic-like) operators obey the commutation relations

$$[a_i, a_j^+] = a_i a_j^+ - a_j^+ a_i = \delta_{ij}. \tag{B.6}$$

This *ansatz* can be used to derive a continuum equation for the cell density. The line of reasoning is as follows. The scalar product is defined as [19]

$$\langle x'_1, \dots, x'_i, \dots | x_1, \dots, x_i, \dots \rangle = x_1! x_2! \dots x_i! \dots x_N! \delta_{x'_1, x_1} \delta_{x'_2, x_2} \dots \delta_{x'_i, x_i} \dots \delta_{x'_N, x_N} \tag{B.7}$$

The  $\delta_{x_i x'_i}$   $i = 1, \dots, N$  result from the orthogonality of the states. From the operator equations (23), (B.3) one can obtain the original master equation by multiplying with the left eigenvector due to

$$\langle x'_1, \dots, x'_i, \dots, x'_N | \partial_t \hat{\Phi}(t) \rangle = \partial_t \langle x'_1, \dots, x'_i, \dots, x'_N | \hat{\Phi} \rangle \tag{B.8}$$

$$= \partial_t \sum_x p(\underline{x}; t) \langle x'_1, \dots, x'_i, \dots | x_1, \dots, x_i, \dots \rangle \tag{B.9}$$

$$= \partial_t \sum_x p(\underline{x}; t) \langle x'_1, \dots, x'_i, \dots | x_1, \dots, x_i, \dots \rangle \tag{B.10}$$

$$= x_1! x_2! \dots x_i! \dots x_N! \partial_t p(\underline{x}'; t). \tag{B.11}$$

In the last step, Eq. (B.7) has been used. Now we are able to express the master equation as a combination of bosonic-like creation and annihilation operators acting on the ground state of the multi-particle system. This representation then allows

us to use the formalism of quantum many particle systems. We choose an initial condition for the master equation to be a multivariate Poissonian [52]

$$p(\{x_i\}; 0) = e^{-N_X(0)} \prod_i \frac{x_{i0}^{x_i}}{x_i!} \tag{B.12}$$

with  $N_X = \sum_i x_{i0}$  (the index “0” denotes  $t = 0$ ).

The representation of the “Hamiltonian”  $H$  for the system of reaction equations (17)–(19) in terms of creation/annihilation operators is

$$\begin{aligned} H = \sum_i & \left\{ \underbrace{\frac{\lambda}{\tilde{N}} [(\tilde{N} - 1)(1 - a_i^+) a_i^+ a_i - (1 - a_i^+) (a_i^+)^2 a_i^2]}_{(1)} \right. \\ & + \sum_j \underbrace{\frac{d_{ij}}{\tilde{N}} [\tilde{N}(a_i^+ - a_j^+) a_i - (a_i^+ - a_j^+) a_j^+ a_j a_i]}_{(2)} \\ & + \sum_j \underbrace{\frac{\omega_{ij}}{\tilde{N}} [\tilde{N}(a_i^+ - a_j^+) a_i - (a_i^+ - a_j^+) a_j^+ a_j a_i]}_{(2)} \\ & \left. + \underbrace{\zeta(1 - a_i^+) a_i}_{(4)} \right\}. \tag{B.13} \end{aligned}$$

Note also that setting  $a_l^+ = 1 \forall l = i, j$  yields  $H = 0$  in agreement with the conservation of probability. The formal solution of Eq. (B.1) is

$$|\hat{\Phi}(t)\rangle = e^{-tH} |\hat{\Phi}(0)\rangle \tag{B.14}$$

$$= \lim_{\Delta t \rightarrow 0} (1 - H\Delta t)^{t/\Delta t} |\hat{\Phi}(0)\rangle, \tag{B.15}$$

where in the last step the Trotter formula has been used.

An observable  $\mathcal{O}(x_1, x_2, \dots)$  can be expressed by

$$\langle \mathcal{O} \rangle = \sum_{\{x_i\}} p(\underline{x}, t) \mathcal{O}(\underline{x}) \tag{B.16}$$

$$= \langle 0 | e^{\sum_i a_i \hat{\mathcal{O}}} \sum_{\{x_i\}} p(\{x_i\}; t) (a_1^+)^{x_1} (a_2^+)^{x_2} \dots (a_i^+)^{x_i} \dots | 0 \rangle \tag{B.17}$$

$$= \langle \hat{\Phi}_0 | \hat{\mathcal{O}} | \hat{\Phi}(t) \rangle \tag{B.18}$$

$$= \langle \hat{\Phi}_0 | \hat{\mathcal{O}} e^{-Ht} | \hat{\Phi}(0) \rangle. \tag{B.19}$$

The introduction of a projection state  $\hat{\Phi}_0$  is necessary since  $\langle \hat{\Phi}(t) | H | \hat{\Phi}(t) \rangle$  (which is used in quantum mechanics, where  $\hat{\Phi}$  denotes the solution of Schrödinger’s wave equation and the probabilities are bilinear in  $\hat{\Phi}$ , i.e.  $\sim \langle \hat{\Phi} | \hat{\Phi} \rangle$ ) would be bilinear in  $\hat{\Phi}$  and hence also bilinear in the probability  $p(\underline{x}, t)$ . The projection operator is  $\langle \hat{\Phi}_0 | = \langle 0 | e^{\sum_i a_i}$ , where  $\langle 0 |$  denotes the vacuum state. Note that this construction

insures the conservation of probability by  $\langle \hat{\Phi}_0 | e^{-Ht} | \hat{\Phi}(0) \rangle = 1$ . Moreover,  $\langle \hat{\Phi}_0 | H = 0$  and  $\langle \hat{\Phi}_0 | \hat{\Phi}(0) \rangle = 1$  [15]. Since  $[e^a a^+] = e^a \leftrightarrow e^a a^+ = (a^+ + 1)e^a$ ,

$$\langle \mathcal{O} \rangle = \langle 0 | \hat{\mathcal{O}} e^{-H(a^+ + 1, a)t} | \tilde{\Phi}(0) \rangle. \tag{B.20}$$

Here,  $|\tilde{\Phi}(0)\rangle = e^{\sum_i a_i} |\hat{\Phi}(0)\rangle$ .

The shifted Hamiltonian from Eq. (B.13) reads

$$\begin{aligned} \hat{H}(a_i^+ + 1, a_i) &= \frac{1}{\tilde{N}} \{ \lambda(\tilde{N} - 1)(-a_i^+)(a_i^+ + 1)a_i - \lambda(-a_i^+)(a_i^+ + 1)^2 a_i^2 \\ &+ \sum_j \tilde{N} d_{ij} (a_i^+ - a_j^+) a_i - d_{ij} (a_i^+ - a_j^+) (a_j^+ + 1) a_j a_i \\ &+ \sum_j \tilde{N} \omega_{ij} a_j^+ (a_i^+ + 1) a_i - \omega_j a_j^+ (a_j^+ + 1) (a_i^+ + 1) a_j a_i \\ &- \tilde{N} \zeta a_i^+ a_{ij} \}, \end{aligned} \tag{B.21}$$

where  $\hat{H}$  denotes the Hamiltonian for lattice site  $i$  such that  $H = \sum_i \hat{H}$ . In order to obtain a path integral representation from this relation, we need to insert a complete set of states at each time slice. A usual choice motivated by quantum harmonic oscillators are coherent states, which are a continuous set of eigenstates of the annihilation operator, i.e.,

$$a_i |\{z\}\rangle = z_i |\{z\}\rangle, \tag{B.22}$$

$$a_i^+ |\{z\}\rangle = z_i^* |\{z\}\rangle. \tag{B.23}$$

Coherent states serve as generating functionals for the energy eigenstates [68]. There are different ways to define the coherent state. The choice of the definition affects the relation for the unity operator and thereby the boundary terms of the path integral. However, eventually they all result in the same stochastic differential equation. The definition that is chosen here follows Ref. 63 and is motivated by the observations that after an appropriate operator shift, the boundary terms drop. We define the coherent state according to

$$|\{z\}\rangle = e^{\sum_i z_i (a_i^+ - 1)} |0\rangle. \tag{B.24}$$

The completeness relation now reads

$$1 = \left( \int \prod_{i=1}^N \frac{dz_i^2}{\pi} e^{-|z_i|^2 + z_i + z_i^*} \right) |\{z\}\rangle \langle \{z\}|, \tag{B.25}$$

where  $dz_i^2 = d\text{Re}(z_i) d\text{Im}(z_i)$ . Any operator average is given by Eq. (B.19). Using the Trotter formula, the operator  $e^{-Ht}$  can be subdivided into  $M$  time slices of length  $\Delta t$ , i.e.  $t = \Delta t M$ :

$$\langle \hat{\Phi}_0 | \hat{\mathcal{O}} e^{-Ht} | \hat{\Phi}(0) \rangle \approx \langle \hat{\Phi}_0 | \hat{\mathcal{O}} (e^{-\Delta t H})^M | \hat{\Phi}(0) \rangle. \tag{B.26}$$

A functional integral representation for the many-body evolution operator may be obtained by inserting the unity operator  $M$ -times using the coherent states  $|z\rangle$  [59]. The calculation can best be demonstrated by looking at a single lattice site, and then generalizing to  $N$  lattice sites. For a single lattice site (for which the index  $i$

can be dropped), one obtains

$$\begin{aligned} & \langle \hat{\Phi}_0 | \hat{\mathcal{O}} (e^{-\Delta t H})^M | \hat{\Phi}(0) \rangle \\ &= \int \left\{ \prod_{k=1}^M \frac{dz_k dz_k^*}{\pi} e^{-|z_k|^2 + z_k + z_k^*} \right\} \langle \hat{\Phi}_0 | \hat{\mathcal{O}} | z_M \rangle \langle z_M | e^{-\Delta t H} | z_{M-1} \rangle \\ & \quad \cdots \langle z_2 | e^{-\Delta t H} | z_1 \rangle \langle z_1 | e^{-\Delta t H} | z_0 \rangle. \end{aligned} \quad (\text{B.27})$$

$k$  is the index for the time slices. If  $N$  lattice sites are taken into account,  $|z_k\rangle \rightarrow |\{z_k\}\rangle$ , where  $\{z_k\} = (z_{1,k}, z_{2,k}, \dots, z_{N,k})$  denotes a coherent state on  $N$  lattice sites at time slice  $k = 1, \dots, M$ . Accordingly,

$$\begin{aligned} & \langle \{\hat{\Phi}_0\} | \hat{\mathcal{O}} (e^{-\Delta t H})^M | \{\hat{\Phi}(0)\} \rangle \\ &= \int \left\{ \prod_{k=1}^M \prod_{i=1}^N \frac{dz_{i,k} dz_{i,k}^*}{\pi} e^{-|z_{i,k}|^2 + z_{i,k} + z_{i,k}^*} \right\} \langle \{\hat{\Phi}_0\} | \hat{\mathcal{O}} | \{z_M\} \rangle \langle \{z_M\} | e^{-\Delta t H} | \{z_{M-1}\} \rangle \\ & \quad \cdots \langle \{z_2\} | e^{-\Delta t H} | \{z_1\} \rangle \langle \{z_1\} | e^{-\Delta t H} | \{z_0\} \rangle. \end{aligned} \quad (\text{B.28})$$

Note that the operator  $\mathcal{O}$  has to be expressed as a function of the coherent states. Since the coherent states at different lattice sites  $i$  are orthogonal, the overlap is given by

$$\langle \{z_k\} | \{z_{k-1}\} \rangle = \prod_{i=1}^N \langle z_{i,k} | z_{i,k-1} \rangle. \quad (\text{B.29})$$

A typical term is (in the limit  $\Delta t \rightarrow 0$ ):

$$\begin{aligned} & \langle \{z_k\} | e^{-\Delta t H(\{a_k^+, \{a_k\})} | \{z_{k-1}\} \rangle \\ & \approx -\langle \{z_k\} | 1 - \Delta t H(\{a_k^+, \{a_k\}) | \{z_{k-1}\} \rangle \\ & = -\langle \{z_k\} | \{z_{k-1}\} \rangle + \Delta t \langle \{z_k\} | H(\{a_k^+, \{a_k\}) | \{z_{k-1}\} \rangle \\ & = -\langle \{z_k\} | \{z_{k-1}\} \rangle (1 - \Delta t H(\{z_k^*, \{z_{k-1}\})) \\ & = -\prod_{i=1}^N \langle z_{i,k} | z_{i,k-1} \rangle (1 - \Delta t H(\{z_k^*, \{z_{k-1}\})) \\ & \approx e^{-\Delta t H(z_k^*, z_{k-1})} \prod_{i=1}^N e^{z_{i,k} z_{i,k-1}^* - z_{i,k-1} - z_{i,k}^*}, \end{aligned} \quad (\text{B.30})$$

where the normal order of the creation and annihilation operators, the relation

$$\langle z_{i,k} | z_{i,k-1} \rangle = e^{z_{i,k} z_{i,k-1}^* - z_{i,k-1} - z_{i,k}^*}, \quad (\text{B.31})$$

and the smallness of  $\Delta t$  have been used.

Furthermore, the operator  $\hat{\mathcal{O}}$  can be expressed in terms of  $a_i$  and  $a_i^+$  in normal order and the  $a_i^+$  set equal to one (since  $\langle \{\hat{\Phi}_0\} | e^{\sum_i a_i} a_i^+ = \langle \{\hat{\Phi}_0\} | e^{\sum_i a_i}$ ); then the coherent states are eigenstates of  $\hat{\mathcal{O}}$  so that  $\langle \{\hat{\Phi}_0\} | \hat{\mathcal{O}} | \{z_M\} \rangle = \mathcal{O} \langle \{\hat{\Phi}_0\} | \{z_M\} \rangle$ . Since the projection state  $|\hat{\Phi}_0\rangle$  is a coherent state with eigenvalue 1:

$$\langle \{\hat{\Phi}_0\} | \{z_M\} \rangle = \langle 0 | e^{\sum_i a_i} e^{\sum_i z_{i,M} (a_{i,M}^+ - 1)} | 0 \rangle \quad (\text{B.32})$$

$$\propto \prod_{i=1}^N e^{-z_{i,M}} e^{z_{i,M}} = 1. \quad (\text{B.33})$$

This can immediately be seen if we again consider one lattice site only, i.e. drop the index  $i$ . The projection state  $\langle \hat{\Phi}_0 | = \langle 0 | e^a$  ( $|\hat{\Phi}_0\rangle = e^{a^+} |0\rangle$ ) is a (not normalized) coherent state with eigenvalue 1 (compare Eq. (B.31)). If this is generalized to many lattice sites, then  $a \rightarrow \sum_i a_i$ .

Hence,

$$\begin{aligned}
 & \langle \{\hat{\Phi}_0\} | \hat{\mathcal{O}} (e^{-\Delta t H})^M | \{\hat{\Phi}(0)\} \rangle \\
 &= \int \left\{ \prod_{i=1}^N \prod_{k=1}^M \frac{dz_{i,k} dz_{i,k}^*}{\pi} \mathcal{O} e^{-\hat{H}(z_{i,k}^*, z_{i,k}) \Delta t} e^{z_{i,k}^* z_{i,k-1} - z_{i,k}^* - z_{i,k-1}} \right. \\
 &\quad \left. \times e^{-z_{i,k} z_{i,k}^* + z_{i,k}^* + z_{i,k}} \right\} \\
 &= \int \left\{ \prod_{k=1}^M \prod_{i=1}^N \frac{dz_{i,k} dz_{i,k}^*}{\pi} \right\} \mathcal{O} e^{\sum_{i=1}^N \sum_{k=1}^M \{-\hat{H}(z_{i,k}^*, z_{i,k}) \Delta t + z_{i,k}^* z_{i,k-1} - z_{i,k}^* - z_{i,k-1}\}} \\
 &\quad \times e^{\sum_{i=1}^N \sum_{k=1}^M \{-z_{i,k} z_{i,k}^* + z_{i,k}^* + z_{i,k}\}} \tag{B.34}
 \end{aligned}$$

$$\begin{aligned}
 &= \int \left\{ \prod_{k=1}^M \prod_{i=1}^N \frac{dz_{i,k} dz_{i,k}^*}{\pi} \right\} \\
 &\quad \times \mathcal{O} e^{\sum_{i=1}^N \left( \sum_{k=1}^M \{-\hat{H}(z_{i,k}^*, z_{i,k}) \Delta t + z_{i,k}^* (z_{i,k-1} - z_{i,k})\} \right) + z_{i,M} - z_{i,0}}, \tag{B.35}
 \end{aligned}$$

where we have used  $|\hat{\Phi}(0)\rangle = |z_0\rangle$ . We have further replaced  $\hat{H}(z_{i,k}^*, z_{i,k-1})$  by  $\hat{H}(z_{i,k}^*, z_{i,k})$  since in the limit  $\Delta t \rightarrow 0$  that we perform below, the difference between these terms only generates terms of higher order in  $\Delta t$  that can be neglected. With the shift  $z_{i,k}^* \rightarrow \bar{z}_{i,k} + 1$ ,

$$\langle \{\hat{\Phi}_0\} | \hat{\mathcal{O}} (e^{-\Delta t H})^M | \{\hat{\Phi}(0)\} \rangle \equiv \int \left\{ \prod_{k=1}^M \prod_{i=1}^N \frac{dz_{i,k} dz_{i,k}^*}{\pi} \right\} \mathcal{O} e^{-S} \tag{B.36}$$

with

$$S = \sum_{i=1}^N \sum_{k=1}^M \bar{z}_{i,k} (z_{i,k} - z_{i,k-1}) + \hat{H}(\bar{z}_{i,k} + 1, z_{i,k}), \tag{B.37}$$

since due to the shift the boundary terms  $\sum_{i=1}^N z_{i,M} - z_{i,0}$  drop. The shifted Hamiltonian now reads (for the next steps until Eq. (B.43), we dropped the index  $k$  for simplicity)

$$\begin{aligned}
 \sum_i \hat{H}(\bar{z}_i + 1, z_i) &= \frac{1}{\tilde{N}} \sum_i \{ \lambda(\tilde{N} - 1)(-\bar{z}_i)(\bar{z}_i + 1)z_i - \lambda(-\bar{z}_i)(\bar{z}_i + 1)^2 z_i^2 \\
 &\quad + \sum_j \tilde{N} d_{ij}(\bar{z}_i - \bar{z}_j)z_i - d_{ij}(\bar{z}_i - \bar{z}_j)(\bar{z}_j + 1)z_j z_i \\
 &\quad + \sum_j \tilde{N} \omega_{ij}(\bar{z}_i - \bar{z}_j)z_i - \omega_{ij}(\bar{z}_i - \bar{z}_j)(\bar{z}_j + 1)z_j z_i - \tilde{N} \zeta \bar{z}_i z_i \}. \tag{B.38}
 \end{aligned}$$

Further,

$$\sum_{ij} d_{ij}(\bar{z}_i - \bar{z}_j)z_i = - \sum_{ij} d_{ij} \bar{z}_i (z_j - z_i) \tag{B.39}$$

$$= - \sum_i \bar{z}_i \sum_e d_{i,i+e} (z_{i+e} - z_i) \tag{B.40}$$

$$= - \sum_i D \bar{z}_i \Delta z_i, \tag{B.41}$$

where  $d_{ij} = d_{ji}$  has been used,  $D$  is the hopping rate between adjacent compartments, and  $\Delta$  the lattice Laplacian. Moreover,

$$\begin{aligned} \sum_{ij} d_{ij}(\bar{z}_i - \bar{z}_j)(\bar{z}_j + 1)z_jz_i &= \sum_{ij} d_{ij}\bar{z}_i(\bar{z}_j + 1)z_jz_i - \sum_{ij} d_{ij}\bar{z}_j(\bar{z}_j + 1)z_jz_i \\ &\stackrel{(A)}{=} - \sum_i \sum_e d_{i,i+e}(z_{i+e} - z_i)(\bar{z}_{i+e} - \bar{z}_i)\bar{z}_iz_i \\ &\quad - \sum_i \sum_e d_{i,i+e}(z_{i+e} - z_i)\bar{z}_iz_i^2 \\ &= - \sum_i (2D\nabla z_i \nabla \bar{z}_i z_i \bar{z}_i + D\bar{z}_iz_i^2 \Delta \bar{z}_i). \end{aligned} \tag{B.42}$$

In (A) we have exchanged the indices  $i \leftrightarrow j$ , set  $j = i + e$  (with  $e = \pm 1$ ), and used  $d_{ji} = d_{ij}$ .  $\sum_e (z_{i+e} - z_i)(\bar{z}_{i+e} - \bar{z}_i) = 2\nabla z_i \nabla \bar{z}_i$  noting that  $(z_{i\pm 1} - z_i) = \pm \nabla z_i$  is a “lattice derivative.” The same can be done for the term  $\propto \omega_{ij}$ .

With the setting  $(z_{i,k} - z_{i,k-1})/\Delta t \xrightarrow{\Delta t \rightarrow 0} \partial z_{i,k}/\partial t$ , one obtains in the limit  $\Delta t \rightarrow 0$ ,  $M \rightarrow \infty$  such that  $M\Delta t = t$  is kept fixed, an action which is continuous in time:

$$\begin{aligned} S &= \int_{t_0}^{t'} \sum_i [\partial_{t'} z_i \bar{z}_i \\ &\quad + \bar{z}_i \{(-\lambda(\tilde{N} - 1 - z_i)z_i + \tilde{N}\zeta z_i - (D + \omega)\tilde{N}\Delta z_i\}/\tilde{N} \\ &\quad + \bar{z}_i^2 \{-\lambda((\tilde{N} - 1) - 2z_i)z_i\}/\tilde{N} \\ &\quad + \{\lambda z^2 \bar{z}^3 + 2(D + \omega)\nabla \bar{z}_i \nabla z_i \bar{z}_i z_i + (D + \omega)\Delta \bar{z}_i z_i^2 \bar{z}_i\}] \frac{1}{\tilde{N}} dt. \end{aligned} \tag{B.43}$$

In the case where the action can be brought into the form

$$S \propto \sum_i \int_{t_0}^{t'} \{ \bar{z}_i f_1(z, \partial_t z, \nabla z, \nabla^2 z, \dots) + \bar{z}_i^2 f_2(z, \nabla z, \nabla^2 z, \dots) \} dt \tag{B.44}$$

the path integral can be performed such that we obtain an exact stochastic differential equation. Here,  $f_1, f_2$  are independent of  $\bar{z}$ . This is not possible in our case, however, as we will see below, a slightly simplified model yields an exact stochastic differential equation with the same mean-field and leading order noise term. We are interested mainly in the large scale properties of the growth process and in the leading order noise contribution. Accordingly, we use power-counting to estimate the contribution of the individual terms [14, 45]. In order to do so, we first cast the action into a continuous form. For this purpose, we set  $z_i(t) \rightarrow b^d n(\underline{r}, t)$ ,  $\bar{z}_i \rightarrow \bar{n}(\underline{r}, t)$ ,  $\Delta \rightarrow b^2 \Delta$ ,  $\sum_i \rightarrow b^{-d} \int d^d x$ . The form of the action then becomes

$$\begin{aligned} S &= \int d^d \underline{r} dt \{ \bar{n}(\hat{\alpha}n + \hat{\beta}n^2 - \hat{D}\Delta n) + \bar{n}^2(\hat{\delta}n + \hat{\gamma}n^2) \\ &\quad + \hat{\theta}n^2 \bar{n}^3 + \hat{\epsilon} \nabla \bar{n} \nabla n \bar{n}_i^2 + \hat{\eta} \Delta \bar{n} n^2 \bar{n} \}. \end{aligned} \tag{B.45}$$

Here, the coefficients with the “ $\hat{\phantom{x}}$ ” are functions of the original coefficients in the action in Eq. (B.43) and the spatial scale  $b$ . We do not need to know them explicitly

in this context. The above form of the action cannot be brought to the form necessary to obtain an “exact” stochastic differential equation that corresponds exactly to the path integral. However, on large lengths and time scales the relevant physics is controlled only by the leading terms in the action which can be identified by dimensional analysis [14, 45, 52]. It is convenient to redefine the fields according to  $\bar{s} = \mu\bar{n}$ ,  $s = \mu^{-1}n$  with  $\mu = \sqrt{\hat{\beta}/\delta}$ , which assigns the same coupling constant to the lowest order non-linearities  $\sim s^2\bar{s}$  and  $\bar{s}^2s$ . With the choice  $[\underline{t}] = k^{-1}$ ,  $[t] = k^2$ ,  $[s\bar{s}] = k^d$ , and  $[s] = k^{d/2}$ ,  $[\bar{s}] = k^{d/2}$ , where  $k$  has the dimension of a wave number, one obtains that the coupling constants of the leading order non-linearities scale as  $\sim k^{(4-d)/2}$ , which is relevant only below the upper critical dimension  $d_c = 4$ . (The choice of relative dimensions of  $s$  and  $\bar{s}$  are somewhat arbitrary; our choice was led by convenience.) The other non-linearities are of higher order and may on large scales be omitted. In fact, the leading order nonlinearities are those of the action known from directed percolation. Here we neglect the higher order-terms and only consider terms up to Gaussian terms  $\propto \hat{n}^2$ . A more systematic analysis would require one to study the effect of the higher order (non-Gaussian) non-linearities by renormalization group theory.

From the above line of reasoning, we find that the action in Eq. (B.43) may be simplified to leading order to the action

$$S \rightarrow \sum_{i=1}^N \int_{t_0}^{t'} \left\{ \partial_t z_i \bar{z}_i + \bar{z}_i \{ -\lambda(\tilde{N} - 1 - z_i)z_i + \tilde{N}\zeta z_i - (D + \omega)\tilde{N}\Delta z_i \} \frac{1}{\tilde{N}} - \frac{\lambda}{\tilde{N}}(\tilde{N} - 1)\bar{z}_i^2 z_i \right\} dt. \tag{B.46}$$

The action has the form in Eq. (B.44), where  $f_2 = -(\tilde{N} - 1)\frac{\lambda}{\tilde{N}}z_i$ .  $e^{-\bar{z}_i(t)^2 f_2 dt}$  can be written as

$$e^{\frac{\lambda}{\tilde{N}}(\tilde{N}-1)\bar{z}_i(t)^2 dt} = \frac{1}{2\pi} \int \mathcal{D}\tilde{\eta}_i e^{-\frac{1}{2}\tilde{\eta}_i(t)^2 - \bar{z}_i \sqrt{2(\tilde{N}-1)}\frac{\lambda}{\tilde{N}}\tilde{\eta}_i \sqrt{dt}}. \tag{B.47}$$

In the same way,

$$e^{\frac{\lambda}{\tilde{N}}(\tilde{N}-1)\sum_i \bar{z}_i(t)^2 dt} = \left(\frac{1}{2\pi}\right)^N \int \prod_i \mathcal{D}\tilde{\eta}_i e^{-\frac{1}{2}\tilde{\eta}_i(t)^2 - \bar{z}_i \sqrt{2(\tilde{N}-1)}\frac{\lambda}{\tilde{N}}\tilde{\eta}_i \sqrt{dt}}. \tag{B.48}$$

This leads to the new path integral:

$$\int \prod_{i=1}^N \left\{ \frac{\mathcal{D}z_i \mathcal{D}\bar{z}_i \mathcal{D}\tilde{\eta}_i}{\pi} \right\} \mathcal{O} e^{\frac{1}{2}\sum_{i=1}^N \int_{t_0}^{t'} -\tilde{\eta}_i(t)^2 dt} e^{-\sum_{i=1}^N \int_{t_0}^{t'} \bar{z}_i(t) f(z_i(t), z_i(t)^2, \dots) dt} \tag{B.49}$$

with

$$f(z_i(t), z_i(t)^2, \dots) dt = \left[ (\partial_t - (D + \omega)\Delta)z_i(t) - \frac{\lambda}{\tilde{N}}(\tilde{N} - 1 - z_i(t))z_i(t) + \zeta z_i(t) \right] dt + \sqrt{2(\tilde{N} - 1)\frac{\lambda}{\tilde{N}}z_i(t)\tilde{\eta}_i \sqrt{dt}}. \tag{B.50}$$

The integration over the  $\bar{z}_i(t)$  can now be performed and the path integral is

$$\propto \int \left\{ \prod_{k=1}^M \prod_{i=1}^N \frac{\mathcal{D}z_i \mathcal{D}\tilde{\eta}_i}{\pi} \right\} \mathcal{O} e^{-\frac{1}{2} \sum_{i=1}^N \int_{t_0}^{t'} \tilde{\eta}_i(t)^2 dt} \delta(f(z_i(t), z_i(t)^2, \dots) dt). \quad (\text{B.51})$$

The integral does not vanish only if  $f(z_i(t), z_i(t)^2, \dots) = 0$ , i.e. if

$$\begin{aligned} dz_i(t) &= \left[ (D + \omega)\Delta z_i(t) + \frac{\lambda}{\tilde{N}}(\tilde{N} - 1 - z_i(t))z_i(t) - \zeta z_i(t) \right] dt \\ &\quad - \sqrt{2(\tilde{N} - 1) \frac{\lambda}{\tilde{N}} z_i(t) \tilde{\eta}_i} \sqrt{dt} \\ &\approx [\lambda(1 - z_i(t)/\tilde{N})z_i(t) - \zeta z_i(t) + (D + \omega)\Delta z_i(t)] dt - \sqrt{2\lambda z_i(t) \tilde{\eta}_i} \sqrt{dt}. \end{aligned} \quad (\text{B.52})$$

For the last step, we assume sufficiently large compartments and  $\tilde{N} \gg 1$  (note that the corresponding terms in mean field equation calculated directly from the “reaction-equations” is also  $\propto \tilde{N}$ ).  $-\tilde{\eta}_i/\sqrt{dt} = dW_i$  is the Wiener increment with  $\langle dW_i(t) \rangle = 0$  and  $\langle dW_i(t) dW_j(t') \rangle = \delta(t - t') \delta_{ij} dt$ . Note that the mean-field term is the same that would also be expected from other methods such as the Poisson-representation of the master equation (for this method, see Ref. 36), or a direct calculation of the expectation values  $\langle x_i \rangle$  followed by a continuum-limit. The stochastic differential equation reflects the fact that the division into neighbor compartments can to lowest order be decomposed into a division within the same department followed by a hopping into an adjacent department.

We now define  $z_i(t) = b^d n(\underline{x}, t)$   $\Delta \rightarrow b^2 \Delta$ , where  $b$  is the lattice spacing. We further set  $\eta(\underline{x}, t) = -\tilde{\eta} b^{-d/2} / dt^{1/2}$  and assume that  $\tilde{N} = b^d / l^d$  (with cell size  $l = 1$ ). Then

$$\frac{\partial n(\underline{x}, t)}{\partial t} = (b^2 D + b^2 \omega) \Delta n(\underline{x}, t) + (\lambda(1 - n(\underline{x}, t)) - \zeta) n(\underline{x}, t) + \sqrt{2\lambda n(\underline{x}, t)} \eta. \quad (\text{B.53})$$

Here,  $\langle \eta(\underline{x}, t) \rangle = 0$ ,  $\langle \eta(\underline{x}, t) \eta(\underline{x}', t') \rangle = \delta(\underline{x} - \underline{x}') \delta(t - t')$ . Now, we re-insert our original parameter choice:

$$\omega = \frac{\lambda}{2d\tilde{b}^2}, \quad (\text{B.54})$$

$$D = \frac{\phi}{2d\tilde{b}^2}, \quad (\text{B.55})$$

and obtain

$$\frac{\partial n(\underline{x}, t)}{\partial t} = l^2 \frac{\lambda + \phi}{2d} \Delta n(\underline{x}, t) + (\lambda(1 - n(\underline{x}, t)) - \zeta) n(\underline{x}, t) + \sqrt{2\lambda n(\underline{x}, t)} \eta. \quad (\text{B.56})$$

A different reaction scheme in which, different from the reaction scheme in Eqs. (17)–(19),  $\bar{\lambda} = \lambda$ ,  $\bar{d}_{ij} = d_{ij}$ ,  $w_{ij} = 0$  and the reaction  $X_i \rightarrow_{\kappa} 2X_i$  is added in order to account for the density limitation yields to an exact stochastic differential equation since for these settings the dynamic action adopts exactly the form in Eq. (B.44). Such a model has been used in Ref. 62 to model chemical reactions.

Comparing this with our model gives a further justification of our approximations. With an appropriate choice of  $\kappa$ , the mean-field part of the resulting stochastic partial differential equation becomes the same as in our approach while the noise term is  $\sqrt{2\lambda n(1-n)}\eta$ . However, this approach is less intuitive than the one we used here since it requires one to put in the space limitation artificially.

## References

- [1] Alt, W., Brettschneider, T. and Müller, R., Interactive movement, aggregation and swarm dynamics, in *Multiscale Modeling*, eds. Alt, J. L. W. and Griebel, M., (Birkhäuser, 2003), pp. 221–241.
- [2] Anderson, A., A hybrid mathematical model of solid tumour invasion: The importance of cell adhesion, *J. Theor. Med.* **22**, 163–186 (2005).
- [3] Aplin, A., Howe, A. and Juliano, R., Cell adhesion molecules, signal transduction and cell growth, *Curr. Op. Cell Biol.* **11**, 737–744 (1999).
- [4] Assoian, R., Anchorage-dependent cell cycle progression, *J. Cell Biol.* **136**, 1–4 (1997).
- [5] Balkovetz, D., Evidence that hepatocyte growth factor abrogates contact inhibition of mitosis in Madin–Darby canine kidney cell monolayers, *Life Sci.* **64**(16), 1393–1401 (1999).
- [6] Batchelor, M. and Henry, B., Limits to eden growth in two and three dimensions, *Phys. Lett. A* **157**(4–5), 229–236 (1991).
- [7] Bertuzzi, A., Fasano, A., Gandolfi, A. and Marangi, D., Cell kinetics in tumor cords studied in a model with variable cell cycle lengths, *Math. Bioscience* **177**, 103–125 (2002).
- [8] Beysens, D., Forgacs, G. and Glazier, J., Cell sorting is analogous to phase ordering in fluids, *Proc. Natl. Acad. Sci. (USA)* **97**(17), 9467–9471 (2000).
- [9] Bramson, M. and Griffeath, D., On the Williams–Bjerknes tumour growth model i, *Ann. Prob.* **9**(2), 173–185 (1981).
- [10] Bru, A., Albertos, S., Subiza, J., Garcia–Arsenio, J. and Bru, I., The universal dynamics of tumor growth, *Biophys. J.* **85**, 2948–2961 (2003).
- [11] Brunet, E. and Derrida, B., Effect of microscopic noise on front propagation, *J. Stat. Phys.* **103**(1/2), 269–280 (2001).
- [12] Byrne, H., King, J., McElwain, D. and Preziosi, L., A two-phase model of solid tumor growth, *Appl. Math. Lett.* **16**(4), 567–573 (2003).
- [13] Cantrell, R. and Cosner, C., Deriving reaction–diffusion models in ecology from interacting particle systems, *J. Math. Biol.* **48**, 187–217 (2004).
- [14] Cardy, J., *Scaling and Renormalization in Statistical Physics* (Cambridge University Press, Cambridge, 1996).
- [15] Cardy, J., Field theory and nonequilibrium statistical mechanics, in *Troisieme cycle de la Physique en Suisse Romande* (1998).
- [16] Chaplain, M., A vascular growth, angiogenesis and vascular growth in solid tumours: The mathematical modelling of the stages of tumour development, *Math. Comput. Modelling* **23**(6), 47–87 (1996).
- [17] Chen, C., Byrne, H. and King, J., The influence of growth-induced stress from the surrounding medium on the development of multicell spheroids, *J. Math. Biol.* **43**, 191–220 (2001).
- [18] Chen, C., Mrksich, M., Huang, S., Whitesides, G. and Ingber, D., Geometric control of cell life and death, *Science* **276**, 1425–1428 (1997).

- [19] Chopard, B. and Droz, M., *Cellular Automata Modeling of Physical Systems* (Cambridge University Press, Cambridge, 1998).
- [20] Conti, S., DeSimone, A., Kohn, R., Müller, S. and Otto, F., Multiscale modeling of materials — The role of analysis, in *Trends in Nonlinear Analysis*, eds. Kirkilionis, M., Krömker, S., Rannacher, R. and Tomi, F. (Springer Verlag, Heidelberg 2003), pp. 375–408.
- [21] DeMasi, A., Luckhaus, S. and Presutti, E., Two-scale hydrodynamic limit for a model of malignant tumor cells, MPI-MIS Preprint **2**, 1–47 (2005).
- [22] Dhont, J., *An Introduction to Dynamics of Colloids* (Elsevier, Amsterdam, 1996).
- [23] Doering, C., Mueller, C. and Smereka, P., Noisy wavefront propagation in the Fisher–Kolmogorov–Petrovsky–Piscounov equation, in *Proc. 3rd Int. Conf. Unsolved Problems of Noise*, National Institutes of Health, Bethesda, USA, ed. Bezrukov (American Institute of Physics, 2003), pp. 523–530.
- [24] Dormann, S. and Deutsch, A., Modeling of self-organized avascular tumor growth with a hybrid cellular automaton, *In Silico Biology* **2**, 0035 (2002).
- [25] Drasdo, D., On selected individual-based approaches to the dynamics of multicellular systems, in *Multiscale Modeling*, eds. Alt, J. L. W. and Griebel, M. (Birkhäuser, 2003), pp. 169–203.
- [26] Drasdo, D. and Hoehme, S., A single-cell based model to tumor growth *in vitro*: Monolayers and spheroids, *Phys. Biol.* **2**, 133–147 (2005).
- [27] Drasdo, D. and Höhme, S., Individual-based approaches to birth and death in avascular tumors, *Math. Comp. Modelling* **37**, 1163–1175 (2003).
- [28] Drasdo, D., Kree, R. and McCaskill, J., Monte-Carlo approach to tissue-cell populations, *Phys. Rev. E* **52**(6), 6635–6657 (1995).
- [29] Drasdo, D. and Löffler, M., Individual-based models on growth and folding in one-layered tissues: Intestinal crypts and blastulation, *Nonl. Anal.* **47**, 245–256 (2001).
- [30] Düchting, W., Ulmer, W. and Ginsberg, T., Cancer: A challenge for control theory and computer modelling, *Europ. J. Cancer* **32A**(8), 1283–1292 (1996).
- [31] Durrett, R. and Levin, S., The importance of being discrete (and spatial), *Theor. Popul. Biology* **46**, 363–394 (1994).
- [32] Eden, M., A two-dimensional growth process, in *Proc. of the 4th Berkeley Symp. Mathematics and Probability*, ed. Neyman, J. (University of California Press, 1961), pp. 223–239.
- [33] Elderfield, D., Field theories for kinetic growth models, *J. Phys. A: Math. Gen.* **18**, L773–L780 (1985).
- [34] Freshney, R., *Culture of Animal Cells* (Alan R. Liss. Inc., New York, 1983).
- [35] Galle, J., Loeffler, M. and Drasdo, D., On the temporal-spatial organization of epithelial cell populations *in vitro*, in *Mathematical Modelling & Computing in Biology and Medicine*, ed. Capasso, V. (Marcel Dekker Inc, 2003), pp. 375–385.
- [36] Gardiner, C. W., *Handbook of Stochastic Methods* (Springer, Berlin, 1990).
- [37] Graner, F. and Glazier, J., Simulation of the differential adhesion driven rearrangement of biological cells, *Phys. Rev. E* **47**(3), 2128–2154 (1993).
- [38] Greenspan, H., On the growth and stability of cell cultures and solid tumors, *J. Theor. Biol.* **56**(1), 229–242 (1976).
- [39] Halpin-Healy, T. and Zhang, Y., Kinetic roughening phenomena, stochastic growth, directed polymers and all that, *Phys. Rep.* **254**, 215 (1995).
- [40] Helbing, D., *Traffic Dynamics* (Springer, Heidelberg, New York, 1997) [in German].
- [41] Helbing, D., Traffic and related self-driven many-particle systems, *Rev. Mod. Phys.* **73**, 1067–1141 (2001).

- [42] Helbing, D., Schweitzer, F., Keltsch, J. and Molnr, P., Active walker model for the formation of human and animal trail systems, *Phys. Rev. E* **56**, 2527–2539 (1997).
- [43] Hogeweg, P., Evolving mechanisms of morphogenesis: On the interplay between differential adhesion and cell differentiation, *J. Theor. Biol.* **203**, 317–333 (2000).
- [44] Honda, H., Tanemura, M. and Yoshida, A., Differentiation of wing epidermal scale cells in a butterfly under the lateral inhibition model—appearance of large cells in a polygonal pattern, *Acta Biotheor.* **48**(2), 121–136 (2000).
- [45] Janssen, H., On the nonequilibrium phase transition in reaction-diffusion systems with an absorbing stationary state, *Phys. B* **42**, 151–154 (1981).
- [46] Jones, A., Byrne, H., Gibson, J. and Dold, J., A mathematical model of the stress induced during avascular tumour growth, *J. Math. Biol.* **40**, 473–499 (2000).
- [47] Kansal, R., Torquato, S., Harsh, G. R., Chiocca, E. A. and Deisboeck, T. S., Simulated brain tumor growth dynamics using a three-dimensional cellular automaton, *J. Theor. Biol.* **203**, 367–382 (2000).
- [48] Klekotka, P., Santoro, S., Ho, A., Dowdy, S. and Zutter M., Mammary epithelial cell-cycle progression via the integrin, *Am. J. Path.* **159**(3), 983–992 (2001).
- [49] Krug, J. and Spohn, D., Kinetic roughening of growing surfaces, in *Solids Far From Equilibrium*, ed. Godreche, C. (Cambridge University Press, Cambridge, 1991).
- [50] Kunz-Schughart, L., Multicellular tumor spheroids: Intermediates between monolayer culture and *in vivo* tumor, *Cell Biol. Int.*, **23**(3), 157–161 (1999).
- [51] Landau, D., *Theory of Elasticity* (Pergamon, 1975).
- [52] Lee, B., Renormalization group calculation for the reaction  $ka \rightarrow 0$ , *J. Phys. A: Math. Gen.* **27**, 2633–2652 (1994).
- [53] Li, L., Backer J., Wong A., Schwanke E., Stewart B. and Pasdar M., Bcl-2 expression decreases cadherin-mediated cell-cell adhesion, *J. Cell Sci.* **116**, 3687–3700 (2003).
- [54] Luckhaus, S. and Triolo, L., The continuum reaction-diffusion limit of a stochastic cellular growth model, *Rend. Mat. Acc. Lincei* **15**, 215–223 (2004).
- [55] Meineke, F., Potten, C. and Loeffler, M., Cell migration and organization in the intestinal crypt using a lattice-free model, *Cell Prolif.* **34**, 253–266 (2001).
- [56] Mikhailov, A., Selected topics in fluctuation kinetics of reactions, *Phys. Rep.* **5&6**, 307 (1989).
- [57] Moreira, J. and Deutsch, A., Cellular automaton models of tumor development: A critical review, *Adv. Complex Syst.* **5**(2–3), 247–267 (2002).
- [58] Mueller-Klieser, W., A review on cellular aggregates in cancer research, *Cancer Res. Clin. Oncol.* **113**(2), 101–122 (1987).
- [59] Negele, J. and Orland, H., *Quantum Many-Particle Systems* (Perseus Books, Reading Massachusetts, 1989).
- [60] Odell, G., Oster, G., Alberch, P. and Burnside, B., The mechanical basis of morphogenesis, *Dev. Biol.* **85**, 446–462 (1981).
- [61] Palsson E. and Othmer H., A model for individual and collective cell movement in dictyostelium discoideum, *Proc. Natl. Acad. Sci. (USA)* **12**(18), 10448–10453 (2000).
- [62] Pechnik, L. and Levine, H., Interfacial velocity corrections due to multiplicative noise, *Phys. Rev. E.* **59**(4), 3893–3900 (1999).
- [63] Peliti, L., Path integral approach to birth-death processes on a lattice, *J. Physique* **46**, 1469–1483 (1985).
- [64] Richardson, D., Random growth in a tessellation, *Proc. Camb. Phil. Soc.* **74**, 515–528 (1973).

- [65] Santini, M., Rainaldi, G. and Indovina, P., Apoptosis, cell adhesion and the extracellular matrix in the three-dimensional growth of multicellular tumor spheroids, *Crit. Rev. Oncol. Hematol.* **36**, 75–87 (2000).
- [66] Schiffer, I., Gebhard, S., Heimerdinger, C., Heling, A., Hast, J., Wollscheid, U., Seliger, B., Tanner, B., Gilbert, S., Beckers, T., Baasner, S., Brenner, W., Spangenberg, C., Prawitt, D., Trost, T., Schreiber, W., Zabel, B., Thelen, M., Lehr, H., Oesch, F. and Hengstler, J., Switching off her-2/neu in a tetracycline-controlled mouse tumor model leads to apoptosis and tumor-size-dependent remission, *Cancer Res.* **63**, 7221–7231 (2003).
- [67] Schnakenberg, J., *Algorithmen in der Quantentheorie und Statistischen Physik* (Zimmermann-Neufang, Ulmen, 1995).
- [68] Serman, G., *An Introduction to Quantum Field Theory* (Cambridge University Press, Cambridge, 1993).
- [69] Stevens, A., The derivation of chemotaxis equations as limit dynamics of moderately interacting stochastic many-particle systems, *Siam J. Appl. Math.* **61**(1), 183–212 (2000).
- [70] Stevens, A., A stochastic cellular automaton modeling of gliding and aggregation of myxobacteria, *Siam J. Appl. Math.* **61**(1), 172–182 (2000).
- [71] Stott, E., Britton, N., Glazier, J. and Zajac, M., Stochastic simulation of benign avascular tumor growth using the potts model, *Math. Comp. Modelling* **30**, 183–198 (1999).
- [72] Stupack, D. and Chersesh, D., Get a ligand, get a life: Integrins, signaling and cell survival, *J. Cell Science* **115**, 3729–3738 (2002).
- [73] Sutherland, R., Cell and environment interactions in tumor microregions: The multicell spheroid model, *Science* **240**, 177–184 (1988).
- [74] Swanson, K., Alvord, E. and Murray, J., Quantitative model for differential motility of gliomas in grey and white matter, *Cell Prolif.* **33**, 317–329 (2000).
- [75] Treiber, M., Hennecke, A. and Helbing, D., Derivation, properties, and simulation of a gas-kinetic-based, non-local traffic model walker model for the formation of human and animal trail systems, *Phys. Rev. E* **59**, 239–253 (1997).
- [76] Warchol, M., Cell density and n-cadherin interaction regulates cell proliferation in the sensory epithelia of the inner ear, *J. Neurosci.* **22**(7), 2607–2616 (2002).
- [77] Ward, J. and King, J., Mathematical modelling of avascular-tumor growth, *IMA J. Math. Appl. Med. Biol.* **14**, 39–69 (1997).
- [78] Williams, T. and Bjerknes, R., Stochastic model for abnormal clone spread through epithelial basal layer, *Nature* **236**, 19–21 (1972).